Ubiquitination-activated TAB–TAK1–IKK–NF-κB axis modulates gene expression for cell survival in the lysosomal damage response

(14 words, 125 characters)

Akinori Endo,[1, 3*] Chikage Takahashi,[1] Yasumasa Nishito,[2] Keiji Tanaka,[1] Yukiko Yoshida[1*]

[1]Laboratory of Protein Metabolism, Tokyo Metropolitan Institute of Medical Science, Tokyo, 156-8506, Japan

[2]Technology Research Division, Tokyo Metropolitan Institute of Medical Science, Tokyo, 156-8506, Japan

[3]Lead contact

[*]Correspondence: endo-ak@igakuken.or.jp (A.E.), yoshida-yk@igakuken.or.jp (Y.Y.)

Abstract

The lysosomal damage response is important for the maintenance of cellular homeostasis. Although the mechanisms underlying the repair and autophagic elimination of damaged lysosomes have been elucidated, the early signal transduction pathways and genes induced in response to lysosomal damage remain elusive. We performed transcriptome and proteome analyses and found that the TAB–TAK1–IKK–NF-κB axis is activated by K63-linked ubiquitin chains that accumulate on damaged lysosomes. This activates the expression of various transcription factors and cytokines that promote anti-apoptosis and intercellular signaling. The findings highlight the crucial role of ubiquitin-regulated signal transduction and gene expression in cell survival and cell–cell communication in response to lysosomal damage. The results suggest that the ubiquitin system is not only involved in the removal of damaged lysosomes by lysophagy, but also functions in the activation of cellular signaling for cell survival.

(140 words)

Introduction

Lysosomes are the primary degradative organelles and play a pivotal role in maintaining cellular and tissue homeostasis[1,2]. Lysosomal dysfunction is associated with various diseases, underscoring the crucial role of lysosomal integrity and its quality control in human health[3-5]. Lysosomes are susceptible to damage by many sources, both internal and external to the cell, which results in the permeabilization and rupture of lysosomal membranes. Crystals, amyloids, pathogens, lipids, lysosomal toxic drugs, and reactive oxygen species (ROS) are among the stressors that can damage lysosomal membranes[6-10]. The release of enzymes and protons from the lumen of damaged lysosomes induces oxidative stress, inflammation, and cell death, which is deleterious to cells and tissues[10,11]. The accumulation of damaged lysosomes is thus an important factor involved in the development of aging-related diseases and other conditions such as crystalline nephropathy, and neurodegenerative and infectious diseases[3-5,12].

To overcome lysosomal damage and restore lysosomal functionality, cells have developed a set of response pathways that is collectively referred to as the lysosomal damage response[6,13]. The quality control mechanisms for damaged lysosomes include repair, elimination, and regeneration. Lysosomal membrane damage triggers the recruitment of the endosomal sorting complex required for transport (ESCRT) to repair the damaged membrane[13,14]. When the damage is extensive and repair is not feasible, the damaged lysosome undergoes autophagic elimination in a process known as lysophagy[13,15]. In lysophagy, lysosomal membrane permeabilization leads to extensive ubiquitination of exposed proteins. This triggers the recruitment of ubiquitin-binding autophagy receptors,

which activates autophagy to sequester and degrade damaged lysosomes[13,16]. Protein ubiquitination is an important form of post-translational modification that is comparable to protein phosphorylation. Protein ubiquitination in lysophagy occurs through the formation of Lys-63 linked ubiquitin chains (K63 ubiquitin)[17]. Substrate ubiquitination in damaged lysosomes is catalyzed by the E2 ubiquitin-conjugating enzyme UBE2QL1 and several ubiquitin E3 ligases, including TRIM16, CUL1–SKP1–FBXO27, and CUL4A–DDB1–WDFY1[18-21].

Transcription factor EB (TFEB), a master regulator of lysosome- and autophagy-related gene expression, is activated during the repair and elimination of damaged lysosomes, which results in the regeneration of lysosomes as part of the lysosomal damage response[22-24]. Under unstimulated conditions, TFEB is phosphorylated by lysosome-associated mTORC1 and binds to 14–3–3 proteins, resulting in the cytoplasmic retention of TFEB[25]. However, lysosomal permeabilization causes the dissociation of mTORC1 from lysosomes, which leads to the dephosphorylation of TFEB and its translocation to the nucleus to activate the expression of lysosome- and autophagy-related genes[3,25].

The elimination of damaged lysosomes through lysophagy requires a period of more than half a day, during which the cell is vulnerable. It is therefore assumed that there are cellular mechanisms that cooperate with lysophagy to maintain cellular health in the lysosomal damage response. In previous work, we demonstrated that K63 ubiquitin, which accumulates on dysfunctional endosomes, induces cytokine production by modulating gene expression in a TGF-beta-activated kinase 1 (TAK1)–TAK1-binding protein (TAB) pathway-dependent manner[26,27]. K63 ubiquitin also accumulates in damaged lysosomes, which serves as an

initiating signal for lysophagy. This prompted us to investigate whether gene expression is induced by ubiquitin-mediated activation of the TAB–TAK1 pathway in the lysosomal damage response, as observed in the endosomal stress response. The transcriptome of cells exposed to lysosomal damaging agents for 30 min has been described[28]; however, genome-wide gene expression patterns associated with the lysosomal damage response remain unclear. In this study, we performed transcriptome and proteome analyses to comprehensively examine the regulation of gene expression in the lysosomal damage response and to identify the underlying signal transduction pathways. We found that accumulation of K63 ubiquitin chains in damaged lysosomes activates the TAB–TAK1–IKK–NF-κB pathway, which in turn induces the expression of various transcription factors and cytokines. We elucidated that the critical role of the TAB–TAK1–IKK–NF-κB pathway in cell survival and intercellular signal transduction. Collectively, the findings suggest the existence of a universal response mechanism against intracellular K63 ubiquitin accumulation.

Results

Lysosomal damage has a global impact on the transcriptome and proteome

To comprehensively investigate the changes in gene expression caused by lysosomal damage, we performed transcriptome analysis and compared mRNA expression between cells treated with L-Leucyl–L-Leucine methyl ester (LLOMe), a well-characterized inducer of lysosomal damage[29], and control cells. We used RPE-1 cells, which are commonly used in aging research. Transcriptome data revealed substantial alterations in gene expression in response to lysosomal damage. We identified >1,000 genes (946 upregulated and 164 downregulated genes from >13,000 transcripts with Log_2 fold change (FC) >|1| and P <0.05) that exhibited significant changes at 2 h after LLOMe treatment (Fig. 1A). Proteome analysis was performed to determine the correlation between proteomic changes and the observed alterations in the transcriptome. The analysis identified 86 upregulated and 60 downregulated proteins (of >10,000 proteins with Log_2 FC >|1| and P <0.05) (Fig. 1B). There was a modest correlation between the significant upregulation at the RNA level and that at the protein level, with a correlation coefficient (R) of 0.5899 from 302 data points (Fig. 1C and Fig. S1A). The representative targets interleukin-1 β (IL1β), IL6, interferon regulatory factor 1 (IRF1), and the proto-oncogenes c-Jun (JUN) and c-Fos (FOS) were upregulated at both the RNA and protein levels (Fig. 1C and S1A, B). This indicates that alterations in the transcriptome were, at least in part, responsible for those observed in the proteome. Genes showing significant upregulation in the transcriptome and proteome analyses were subjected to gene enrichment analysis using the Gene Ontology Molecular Function (GOMF) reference dataset (Fig. 1D, E). The results showed that these genes were primarily enriched in transcription factors and

cytokines (labeled in red and blue, respectively, in Fig. 1D). Analysis using a Molecular Signatures Database (MSigDB) hallmark gene set[30], a phenotypic reference dataset, indicated that genes upregulated at both the RNA and protein levels were involved in biological regulatory processes including the inflammatory response and apoptosis (Fig. 1E). It is noteworthy that the transcription factor prediction using the DoRothEA regulon[31,32] identified the p65 (RELA) and p105 (NFKB1) subunits of the NF-κB family as the primary transcription factors regulating gene expression in the lysosomal damage response (Fig. 1F). This suggests that NF-κB activation is involved in the regulation of gene expression in the lysosomal damage response. The upregulation of IL1β, IL6, IRF1, JUN, and FOS at the protein level was confirmed by immunoblotting (Fig. 1G).

Taken together, the results suggest that in the lysosomal damage response, the proteome is remodeled according to alterations in the transcriptome; this remodeling is mediated primarily through NF-κB and involves many transcription factors and cytokines, which may potentially lead to the regulation of inflammation and apoptosis (Fig. 1H).

Lysosomal damage activates TAK1 in a ubiquitin- and TAB-dependent manner

Lysosomal membrane damage exposes proteins such as galectin-3 (Gal-3), and these proteins are extensively ubiquitinated by ubiquitin ligases, resulting in the accumulation of ubiquitinated proteins within damaged lysosomes[20,21,33]. An endosomal stress response mechanism was recently described whereby K63 ubiquitin accumulates on dysfunctional endosomes, activating TAK1 in a TAB-dependent manner[26]. TAB2 and TAB3 (a paralog of TAB2) function as ubiquitin decoders that specifically recognize K63 ubiquitin via the C-

terminal Npl4 zinc finger (NZF) domain[34,35]. The finding that TAB binding to unanchored K63 ubiquitin chains is sufficient to activate TAK1 in vitro[36] suggest that the conjugation of K63 ubiquitin to bulky substrates on endosomes is sufficient to facilitate TAB-dependent TAK1 activation. This prompted us to investigate whether the accumulation of K63 ubiquitin in other regions of the cytoplasm also results in TAK1 activation. TAK1 controls the function of the p62/sequestosome, an autophagy receptor, and TAB2 undergoes TRIM38-mediated lysosomal degradation in response to lysosomal damage[37,38]. However, whether TAK1 is activated in a TAB-dependent manner and the role of the TAB–TAK1 signaling pathway in the lysosomal damage response remain unanswered questions.

To determine whether the TAB–TAK1 signaling pathway is activated in response to lysosomal damage, we initially examined the subcellular localization of TAB2 and TAK1. The recruitment of Gal-3 and K63 ubiquitin to damaged lysosomes was confirmed in RPE-1 cells (Fig. S2A-B). The co-localization of TAB2 and TAK1 with K63 ubiquitin in damaged lysosomes was observed 5 min after LLOMe treatment (Fig. 2A). Immunoblotting analysis showed that the accumulation of K63 ubiquitin in the cell was accompanied by an increase in active phosphorylated TAK1, which was first detected 5 min after LLOMe treatment (Fig. 2B). TFEB isolated from cells treated with LLOMe exhibited a downshift on the gel, which is a characteristic of TFEB activation[39]. This indicates that a lysosomal damage response was activated under these experimental conditions (Fig. 2B). TAK1 activation was abolished by the E1 ubiquitin-activating enzyme inhibitor TAK-243 and depletion of TAB2 and TAB3 (Fig. 2C, D). These results suggest that TAK1 is activated in a ubiquitin- and TAB-dependent manner in the lysosomal damage response.

The TAB–TAK1 pathway plays a pivotal role in the induction of cytokines and transcription factors in the lysosomal damage response

To gain further insight into the involvement of the TAB–TAK1 pathway in the regulation of gene expression associated with the lysosomal damage response, an additional transcriptome analysis was performed on TAB- and TAK1-depleted cells treated with LLOMe for 2 h. The genes upregulated in response to lysosomal damage were classified into six distinct clusters within the dataset (Fig. 3A). Clusters 4 and 5 comprised genes that are expressed in a TAB- and TAK1-dependent manner (Fig. 3A). Most of the genes upregulated in a TAB- and TAK1-dependent manner showed overlapping expression patterns (Fig. S3A, B); these genes were enriched for cytokines and growth factors, and their functions were linked to inflammatory responses and apoptosis, as shown in the gene enrichment analysis (Fig. S3C, D). Transcription factor prediction based on the DoRothEA regulon indicated that genes in cluster 4, whose expression was inhibited by depletion of TAB and TAK1, were targets of the NF-κB family, including RelA, NFKB1, and c-Rel (REL) (Fig. 3B). The NF-κB family members were identified as the primary transcription factors regulating gene expression in the lysosomal damage response (Fig. 1F). This indicates that the TAB–TAK1 pathway serves as a primary axis for the activation of NF-κB in the lysosomal damage response, thereby inducing target gene expression. Cytokines and growth factors were enriched in cluster 4, and transcription factors were enriched in cluster 5, in which gene expression was partially suppressed (Fig. 3C, E). Regulators of the inflammatory response and apoptotic functions were commonly enriched in clusters 4 and 5 (Fig. 3D). The results of immunoblotting showed

that the protein expression of IL1β, IL6, IRF1, homeobox protein Nkx-3.1 (NKX3.1), and JUN was consistent with the TAB- and TAK1-mediated gene expression. Conversely, depletion of TAB and TAK1 did not affect the expression of FOS at both the mRNA and protein levels (Fig. 3F and S3E). Furthermore, the downshift of TFEB, which indicates the activation of TFEB, was not affected by depletion of TAB and TAK1 (Fig. 3F). This suggests that TFEB activation is independent of the TAB–TAK1 pathway in the lysosomal damage response.

In conclusion, transcriptome analysis in TAB- and TAK1-depleted cells indicates that the TAB–TAK1 pathway induces the expression of cytokines and transcription factors, potentially via NF-κB, in the lysosomal damage response, thereby regulating inflammatory responses and apoptosis.

The K63Ub–TAB–TAK1–IKK–NF-κB pathway is activated in the lysosomal damage response

To elucidate the downstream cascade of the TAB–TAK1 signaling pathway in the early response to lysosomal damage, we performed proteome and phosphoproteome analyses using the TAK1 inhibitor HS-276 (Fig. 4A, S4A). The phosphoproteome analysis showed that the phosphorylation levels of stress-induced mitogen-activated protein kinases (MAPKs), specifically p38α (MAPK14, pT180/pY182) and JNK3 (MAPK10, pY223), as well as MK2 (MAPKAPK2, pT334), a downstream target of MAPKs, increased in response to lysosomal damage, and this increase was dependent on TAK1 (Fig. S4B, C). Phosphorylation of T180/Y182 in p38α and Y223 in JNK3 activates the kinase function[40,41]. The TAK1-

dependent phosphorylation of Y223 in JNK3 in the lysosomal damage response was consistent with a previous report that lysosome rupture activates the TAK1–JNK pathway in THP-1 cells[42]. Additionally, T334 of MK2 is a primary site of phosphorylation by MAPKs[43]. These findings suggest that lysosomal damage induces TAK1-dependent activation of MAPKs. Proteome analysis showed that the inhibitor of NF-κB α (IκBα) undergoes TAK1-dependent degradation 30 min after LLOMe treatment (Fig. 4A, B). The inhibitor of NF-κB kinase (IKK) complex, which comprises IKKα, β, and γ, functions downstream of TAK1 and phosphorylates IκBα, thereby inducing its degradation[44]. Similarly, in response to ubiquitin-mediated endosomal stress, the NF-κB pathway is activated in an IKK-dependent manner[26]. The degradation of IκBα is a hallmark phenomenon upstream of NF-kB activation[45], which is primarily triggered by IKK-mediated phosphorylation. This leads to the hypothesis that the IKK complex activated by the TAB–TAK1 pathway promotes the phosphorylation of IκBα, which leads to its degradation and NF-κB activation in the lysosomal damage response.

We therefore sought to characterize the kinase cascade that is activated in the lysosomal damage response. We confirmed the phosphorylation and subsequent degradation of IκBα (Fig. 4C). We also found that MAPKs and IKK were activated concomitant with a notable phosphorylation of IKK, JNK, and p38, and a relatively minimal phosphorylation of ERK (Fig. 4C). The increase in the phosphorylation levels of IKK, JNK, p38, and IκBα occurred in a ubiquitin-dependent manner, as the induction was abolished by TAK-243 (Fig. 4D). Depletion of TAB, TAK1, and IKK suppressed IκBα phosphorylation, whereas the phosphorylation of JNK and p38 was TAB- and TAK1-dependent (Fig. 4E, F). These findings indicate that the phosphorylation of IκBα is induced in a TAB–TAK1–IKK pathway-

dependent manner. Additionally, it can be postulated that MAPKs, including JNK and p38, are activated by the TAB–TAK1 pathway.

These results collectively suggest that the IKK complex, which is activated by the TAB–TAK1 pathway in response to lysosomal damage, induces the phosphorylation and degradation of IκBα, potentially leading to the activation of NF-κB (Fig. 4G).

The K63Ub–TAB–TAK1–NF-κB pathway regulates the expression of cytokines and transcription factors essential for cell survival and intercellular signaling

IL1β, IL6, IRF1, and NKX3.1 expression was associated with the lysosomal damage response and dependent on the TAB–TAK1 pathway (Fig. 3E, F and S3E). The expression of these genes was suppressed by treatment with TAK-243 and HS-276 (Fig. 5A, B). Depletion of IKKs suppressed target gene expression (Fig. 5C). These findings demonstrate that the expression of these genes is induced by the ubiquitin-dependent activation of the TAB–TAK1–IKK pathway in the lysosomal damage response.

Gene enrichment based on the results of transcriptome and proteome analyses indicated that TAB–TAK1 pathway-dependent gene expression plays a role in the regulation of apoptosis and the inflammatory response (Fig. 3D and S3D). We thus examined the impact of the K63Ub–TAB–TAK1–IKK–NF-κB pathway on these cellular functions. Lysosomal damage for 8 h did not induce apoptosis; however, inhibition of ubiquitination by TAK-243 dramatically induced apoptosis in HeLa and RPE-1 cells (Fig. 5D, S5A). This indicates that ubiquitination is essential for cell survival in the lysosomal damage response. Similarly, inhibition of TAK1 by HS-276 and depletion of TAB, TAK1, and IKKs following lysosomal

damage for 24 h promoted apoptosis in HeLa cells (Fig. 5D-F). TAK1 inhibition induced apoptosis in RPE-1 cells to a lesser extent compared to HeLa cells (Fig. 5D, S5A). These findings demonstrate that the K63Ub–TAB–TAK1–IKK–NF-κB pathway exerts anti-apoptotic effects in response to lysosomal damage, thereby promoting cell survival.

We further investigated the potential autocrine/paracrine-like effects of cytokines such as IL1β and IL6, which are expected to be secreted outside the cells due to their upregulation in the lysosomal damage response. IL6 activates the JAK–STAT pathway, which is accompanied by the phosphorylation of STAT3[46]. Stimulation of untreated cells with culture media from lysosome-damaged cells resulted in the phosphorylation of STAT3, which indicates kinase activation (Fig. 5G). These results suggest that the lysosomal damage response activates intercellular signaling involving the JAK–STAT pathway. Furthermore, the capacity to activate this intercellular signaling was decreased by depletion of TAB, TAK1, and IKKs (Fig. 5H, I).

Collectively, these findings suggest that the K63Ub–TAB–TAK1–IKK–NF-κB pathway plays a pivotal role in cell survival and intercellular signaling in response to lysosomal damage.

Discussion

In this study, comprehensive analyses of the transcriptome and proteome demonstrated that lysosomal damage causes substantial alterations in gene expression, leading to proteome remodeling. Furthermore, we identified the signal transduction pathway mediating this response (Fig. 6). The accumulation of K63 ubiquitin in damaged lysosomes activates the TAB–TAK1–IKK–NF-κB pathway, which induces the expression of various transcription factors and cytokines. The present findings suggest that ubiquitin-dependent signaling pathway play a regulatory role in cell survival and intercellular signaling in the lysosomal damage response.

Prior to this study, our understanding of the lysosomal damage response was largely limited to the processes of repair and elimination of damaged lysosomes, as well as the activation and function of TFEB in lysosomal regeneration. Recent findings highlighting the role of stress granule formation in the lysosomal damage response suggest that additional pathways are involved in this process beyond what was previously anticipated[28]. Nevertheless, the complete picture remains to be elucidated. This study provides new information on the regulation of gene expression and signal transduction in the lysosomal damage response that offers a novel perspective for future research.

Aberrations in the lysosomal damage response are relevant to the pathogenesis of various age-related diseases including neurodegenerative diseases[3,47]. In the context of pathology, inflammation, which is associated with numerous diseases, is linked to lysosomes. The inflammatory response is not only regulated by lysosomal function, but also triggered by lysosomal damage, and observed in lysosomal storage diseases[48,49]. The NLRP3

inflammasome induces an inflammatory response to lysosomal damage by increasing cytokine processing at the protein level[49,50]. The ubiquitin-regulated gene expression of pro-inflammatory cytokines such as IL1β and IL6 may be involved in the induction of inflammation in the lysosomal damage response, in addition to the regulation at the stage of precursor processing. The present data on the regulation of gene expression by ubiquitin-mediated signal transduction may help elucidate the molecular mechanisms underlying diseases associated with lysosome dysfunction.

In this study, we demonstrated the pivotal role of the ubiquitin system in regulating gene expression in the lysosomal damage response, which extends its function beyond that in lysophagy initiation. We found that activation of the TAB–TAK1–IKK–NF-κB pathway, potentially by the accumulation of K63 ubiquitin in damaged lysosomes, and the subsequent induction of gene expression are crucial for cell survival and cell–cell communication in cultured cells. Further analysis is required to determine the impact of this action on disease pathogenesis and the maintenance of cellular homeostasis in organisms.

Related to the present findings, a recent study demonstrated that linear ubiquitin chains formed by LUBAC and deubiquitinated by OTULIN activate NF-κB in the lysosomal damage response[51]. NF-κB activation is essential for cell survival in this biological context. Activated STING at the Golgi also leads to NF-κB activation through LUBAC-mediated formation of linear ubiquitin chains[52]. In addition, the IKK complex is recruited to damaged mitochondria, potentially through its association with accumulated ubiquitin chains, and activates NF-κB[53]. Although the involvement of the TAB–TAK1 pathway was not examined in these studies, a common mechanism underlying NF-κB activation induced by the

accumulation of ubiquitin on damaged or stressed organelles may serve as a unifying determinant. Taken together with our previous findings that K63 ubiquitin accumulation in dysfunctional endosomes induces cytokine expression via the TAB–TAK1 pathway[26], the present results suggest the existence of a universal response to intracellular K63 ubiquitin accumulation resulting from fluctuations in the cellular environment, including organelle stress. This universal response would entail the activation of NF-κB and the modulation of downstream target gene expression for the regulation of cellular functions that maintain homeostasis.

Materials and methods

Cell culture

RPE-1 cells were cultured at 37°C under 5% CO_2 in Dulbecco's Modified Eagle Medium (DMEM) / Ham's F-12 (WAKO, 048-29785) supplemented with 10% fetal bovine serum (FBS, Nichirei, 175013), 1 mM sodium pyruvate (Thermo Fisher Scientific, 11360070), 1× nonessential amino acids (Thermo Fisher Scientific, 11140050), and 1× Penicillin–Streptomycin–Glutamine (Thermo Fisher Scientific, 10378016). HeLa cells were cultured at 37°C under 5% CO_2 in DMEM (Thermo Fisher Scientific, D5796) supplemented with 10% FBS, 1 mM sodium pyruvate, 1× nonessential amino acids, and 1× Penicillin–Streptomycin–Glutamine. For experiments using conditioned medium, RPE-1 cells were stimulated with culture medium from RPE-1 cells that had been treated with or without 1 mM LLOMe (Cayman, 16008). At 30 min after treatment, the LLOMe was washed out and cell were further incubated in DMEM supplemented with 0.5% FBS, 1 mM sodium pyruvate, 1× nonessential amino acids, and 1× Penicillin–Streptomycin–Glutamine for 8 h.

Reagents and inhibitors

To induce lysosomal damage, cells were treated with 1 mM LLOMe for the indicated times. In the event of a longer incubation period, the LLOMe was washed out 2 h after treatment. The following inhibitors were used in this study: TAK-243 (10 μM, Active Biochem, A-1384), and HS-276 (10 μM, Sigma-Aldrich, SML-3629).

Transcriptome analysis

Total RNA from RPE-1 cells was prepared using the Qiashredder kit (Qiagen, 79654), the RNeasy kit (Qiagen, 74104), and DNase treatment (Qiagen, 79254). The quality of RNA samples was assessed using an Agilent 2100 bioanalyzer (Agilent Technologies); an RNA integrity number >9 was recorded for all samples. A total of 500 ng of each sample was processed with the Illumina Stranded mRNA Prep kit, and indexes were added with the IDT for Illumina RNA UD Indexes Set A (Illumina). The average library size was estimated using the Agilent 2100 Bioanalyzer, and libraries were quantified using a Qubit Fluorometer (Thermo Fisher Scientific). Samples were pooled into a single library and sequenced using the NextSeq 1000/2000 P2 Reagents (300 cycles, paired-end 150bp) on the Illumina NextSeq 1000 system. Sequence data were analyzed using the onboard DRAGEN RNA Pipeline Application (v.3.10.12).

Proteome analysis

RPE-1 cells were treated with or without 1 mM LLOMe for the indicated times and then lysed in 5% SDS lysis buffer [5% SDS and 50 mM triethylammonium bicarbonate (TEAB, Thermo Fisher Scientific, 90114)] followed by sonication with an ultrasonication probe. Cell lysates were reduced and alkylated with 4.5 mM dithiothreitol (DTT, Thermo Fisher Scientific, A39255) for 30 min at 55°C and 10 mM iodoacetamide (IAA, Thermo Fisher Scientific, A39271) for 15 min at room temperature (RT). Subsequently, 30 µg of cell lysates were loaded onto S-Trap micro columns (ProtiFi, C02-micro); trypsin and lysyl-endopeptidase (Lys-C) solution (1:10 w/w, Thermo Fisher Scientific, A41009) was added and incubated for 16 h at 37°C. The eluted peptides were dried in a vacuum concentrator and resuspended in 0.1% trifluoroacetic acid (TFA). Aliquots containing 500 ng of peptides from

each sample were loaded onto a Vanquish Neo UHPLC system-connected Orbitrap Exploris 480 mass spectrometer (Thermo Fisher Scientific). The peptides were separated on an analytical column (C18, 1.7 µm particle size × 75 µm diameter × 600 mm, IonOpticks, AUR3-60075C18) heated at 55°C in a column oven (Sonation, PRSO-C2) with a constant flow rate of 250 nL/min. The peptides were eluted with a 0–40% acetonitrile gradient over 120 min. Peptide ionization was performed using the Nanospray Flex Ion Source (Thermo Fisher Scientific). The Orbitrap Exploris 480 mass spectrometer was operated in data-independent acquisition (DIA) mode using a full scan (m/z range of 380–985, nominal resolution of 60,000, and target value of 3×10^6 ions) followed by DIA-MS scans (fixed collision energy of 30%, isolation width of 10 m/z with an overlapping of 1 m/z, nominal resolution of 15,000, and target value of 2×10^6 ions).

DIA-MS data processing and visualization

The MS raw files were searched against the human UniProt reference proteome (Uniprot ID: UP000005640, reviewed, canonical, 20,563 entries) in library-free mode using DIA-NN software (version 1.9.1)[54]. The parameters that differed from the default settings were as follows: variable modifications, oxidation of methionine and acetylation of the peptide N-terminus; precursor m/z range, 380–985. Following processing with DIA-NN, the exported data were subjected to imputation using Perseus software[55]. The default setting was used assuming that missing values represent low protein abundance. In this case, missing values were replaced by random numbers drawn from a normal distribution across the entire matrix.

Gene enrichment tests and clustering were performed using the RNAseqChef software[56], and heatmaps were generated using the Morpheus platform (https://software.broadinstitute.org/morpheus/). The volcano plots, scatter plots, and bar graphs were visualized using GraphPad Prism software (version 8.1.0, GraphPad).

Cell lysis and immunoblotting

Cells were lysed with 2% SDS lysis buffer (2% SDS, 20 mM HEPES pH 7.5, 1 mM EDTA) containing a complete protease inhibitor cocktail (EDTA-free, Roche, 05056489001) and a phosphatase inhibitor cocktail (Roche, 4906845001). Cell lysates were boiled in 1× LDS NuPAGE sample buffer (Thermo Fisher Scientific, NP0008) for 10 min at 70°C, and then electrophoresed on 4–12% NuPAGE Bis-Tris gels (Thermo Fisher Scientific). Proteins were transferred to polyvinylidene difluoride membranes (Millipore, IPVH00010 or Pall, EH-2222). The membranes were incubated with 5% nonfat milk for 1 h at RT, followed by incubation for 2 h at RT with primary antibodies. The primary antibodies used for immunoblotting were anti-IL1β mouse monoclonal (Cell Signaling Technology, 12242), anti-IL6 rabbit monoclonal (Cell Signaling Technology, 12153), anti-IRF1 rabbit monoclonal (Cell Signaling Technology, 8478), anti-NKX3.1 rabbit monoclonal (Cell Signaling Technology, 92998), anti-c-Fos rabbit monoclonal (Cell Signaling Technology, 2250), anti-c-Jun rabbit monoclonal (Cell Signaling Technology, 9165), HRP-conjugated anti-α-tubulin rabbit polyclonal (MBL, PM054-7), anti-K63 ubiquitin rabbit monoclonal (Millipore, 05-1308), anti-ubiquitin mouse monoclonal (Santa Cruz Biotechnology, sc-8017), anti-phospho-TAK1 (T184/T187) rabbit monoclonal (Cell Signaling Technology, 4508), anti-TAK1 rabbit

polyclonal (Cell Signaling Technology, 4505), anti-TAB2 rabbit polyclonal (Abcam, ab222214), anti-TAB3 rabbit polyclonal (Abcam, ab85655), anti-TFEB rabbit monoclonal (Cell Signaling Technology, 37785), anti-phospho-IKKα/β (S176/S180) rabbit monoclonal (Cell Signaling Technology, 2697), anti-IKKα rabbit polyclonal (Cell Signaling Technology, 2682), anti-IKKβ rabbit monoclonal (Cell Signaling Technology, 8943), anti-phospho-IκBα (S32) rabbit monoclonal (Cell Signaling Technology, 2859), anti-IκBα rabbit monoclonal (Cell Signaling Technology, 4812), anti-phospho-JNK (T183/Y185) rabbit monoclonal (Cell Signaling Technology, 4668), anti-JNK rabbit polyclonal (Cell Signaling Technology, 9252), anti-phospho-p38 (T180/Y182) rabbit polyclonal (Cell Signaling Technology, 9211), anti-p38 rabbit monoclonal (Cell Signaling Technology, 8690), anti-phospho-ERK (T202/Y204) rabbit monoclonal (Cell Signaling Technology, 4370), anti-ERK rabbit monoclonal (Cell Signaling Technology, 4695), anti-cleaved caspase-3 rabbit polyclonal (Cell Signaling Technology, 9661), anti-phospho-STAT3 (Y705) rabbit monoclonal (Cell Signaling Technology, 9145), and anti-STAT3 rabbit monoclonal (Cell Signaling Technology, 4904). The membranes were then incubated with secondary antibodies for 50 min at RT. The secondary antibodies used were HRP-conjugated goat anti-rabbit Ig (Promega, W4011) and anti-mouse Ig (Promega, W4021). The antibodies were diluted with Can Get Signal Solutions (TOYOBO, NKB-101). Chemiluminescence images were developed using the ECL Prime Western Blotting Detection Reagent (Cytiva, RPN2236), and acquired with a Fusion FX7 (Vilber Bio Imaging).

Phosphoproteome analysis

RPE-1 cells were treated with or without 1 mM LLOMe and 10 μM HS-276 for the indicated times, after which they were lysed, reduced, and alkylated as described above (proteome analysis). Aliquots containing 200 μg of lysate were loaded onto S-Trap mini columns (ProtiFi, C02-mini), followed by addition of the trypsin solution (1:10 w/w, Cell Signaling Technology, 56296) and incubation for 16 h at 37°C. The eluted peptides were dried in a vacuum concentrator. Phosphopeptides were enriched using the High-Select Fe-NTA Phosphopeptide Enrichment Kit (Thermo Fisher Scientific, A32992) and dried in a vacuum concentrator. The resultant peptides were cleaned using C18 spin tips (Thermo Fisher Scientific, 84850), dried in a vacuum concentrator, resuspended in 0.1% TFA, and loaded onto a Vanquish Neo UHPLC system-connected Orbitrap Exploris 480 mass spectrometer. The peptides were separated on an analytical column (C18, 1.7 μm particle size × 75 μm diameter × 250 mm, IonOpticks, AUR3-25075C18) heated at 55°C in a column oven with a constant flow rate of 250 nL/min. The peptides were eluted with a 0–40% acetonitrile gradient over 120 min. Peptide ionization was performed using the Nanospray Flex Ion Source. The Orbitrap Exploris 480 mass spectrometer was operated in data-dependent acquisition (DDA) mode utilizing a full scan (m/z range, 375–1500; nominal resolution, 60,000; target value, 3×10^6 ions) followed by MS/MS scans (fixed collision energy, 30%; isolation width, 1.6 m/z; nominal resolution, 15,000, and target value, 1×10^5 ions). Precursor ions selected for fragmentation (charge state 2–6) were placed on a dynamic exclusion list for 20 s. A “1-s cycle” DDA method was used, whereby the most intense ions were selected every second for MS/MS fragmentation by higher-energy collisional dissociation.

DDA-MS data processing and visualization

The MS raw files were searched against the human UniProt reference proteome (Uniprot ID: UP000005640, reviewed, canonical, 20,563 entries) using the Sequest HT search program in Proteome Discoverer 3.1 (Thermo Fisher Scientific). Intensity-based non-label quantification was performed using the Precursor Ions Quantifier node in Proteome Discoverer 3.1. Volcano plots, scatter plots, and bar graphs were visualized using GraphPad Prism (version 8.1.0, GraphPad).

Immunofluorescence and confocal microscopy analysis

Cells were plated in 35-mm glass-bottomed dishes coated with poly-L-lysine (MatTek, P35-GC-0-10-C). They were fixed with 4% paraformaldehyde in PBS for 10 min at RT and permeabilized with 0.2% Triton X-100 in PBS for 5 min at RT. Alternatively, the cells were incubated with ice-cold methanol for 10 min on ice. Following incubation with 5% FBS and 0.1% Tween in PBS for 30 min at RT, cells were incubated with primary antibodies for 2 h at RT and then stained with secondary antibodies and DAPI (Thermo Fisher Scientific, D1306) for 1 h at RT. The following primary antibodies were used: anti-TAB2 mouse monoclonal (Santa Cruz Biotechnology, sc-398188), anti-LAMP1 rabbit monoclonal (Cell Signaling Technology, 9091), anti-K63 ubiquitin rabbit monoclonal (Millipore, 05-1308), anti-TAK1 mouse monoclonal (Santa Cruz Biotechnology, sc-7967), and anti-Galectin-3 rat monoclonal (Santa Cruz Biotechnology, sc-23938). The following secondary antibodies were

purchased from Thermo Fisher Scientific: Alexa Fluor 488-conjugated anti-mouse (A-11029) and anti-rat (A-11006); and Alexa Fluor 594-conjugated anti-rabbit (A-11012). After staining, the cells were coverslipped (Matsunami, C015001) with SlowFade Gold (Thermo Fisher Scientific, S36936). Images were captured using ZEN 3.8 imaging software and LSM980 laser-scanning confocal microscopes equipped with a Plan-Apochromat 63×/1.4NA oil lens (Carl Zeiss).

Small interfering RNA (siRNA) transfection

Cells were transfected with siRNAs using Lipofectamine RNAiMax (Thermo Fisher Scientific) at a final siRNA concentration of 30 nM. Cells were harvested and analyzed 72 h after transfection with siRNA. The siRNAs utilized pools of four different sequences (Thermo Fisher Scientific). The following siRNAs were used: TAB2 siRNAs: L-004771; TAB3 siRNAs: L-015572; TAK1 siRNAs: L-003790; IKKα siRNAs: L-003473; IKKβ siRNAs: L-003503; and IKKγ siRNAs: L-003763.

RT-qPCR analysis

Total RNA was extracted using NucleoSpin RNA Plus (MACHEREY-NAGEL, 740984.250). cDNA was generated using the ReverTra Ace qPCR RT Master Mix with gDNA Remover kit (TOYOBO, FSQ-301). Quantification of mRNA was performed using a Light Cycler 480 (Roche) with THUNDERBIRD SYBR qPCR Mix (TOYOBO, QPS-201) as the detection reagent. The primer sets used for qRT-PCR were as follows: IL1β forward: TACGATCACTGAACTGCACGC, IL1β reverse: CTTGTTGCTCCATATCCTGTCCC;

IL6 forward: TCATCACTGGTCTTTTGGAGTTTG, IL6 reverse: CAGCTCTGGCTTGTTCCTCAC; IRF1 forward: GCCATTCACACAGGCCGATAC, IRF1 reverse: TGCTCTGGTCTTTCACCTCCTC; NKX3.1 forward: CTGGGAGACTTGGAGAAGCAC, NKX3.1 reverse: GGATAGCTGTTATACACGGAGACC; and GAPDH forward: AGAAGGTGGTGAAGCAGGCG, GAPDH reverse: CAAAGTGGTCGTTGAGGGCAATG.

Statistical analysis

Statistical analysis was performed using GraphPad Prism (version 8.1.0). All statistical information is provided in the figure legends. First, the sample distribution was assessed using the Shapiro–Wilk test. In the absence of formal testing, datasets with small sample sizes were assumed to have normal distribution. The unpaired two-tailed Student's t-test was used to determine statistical significance when comparing unpaired two independent groups with normal distribution and no significant difference in standard deviation (SD). For multiple comparisons involving more than two unpaired groups with normal distribution, an ordinary one-way ANOVA with Dunnett's multiple comparison test was used. In all instances, statistical significance was evaluated with a 95% confidence interval, and a P value <0.05 was considered statistically significant.

Data availability

The RNA sequencing data have been deposited with links to BioProject accession number PRJDB19809 in the BioProject database of DNA Data Bank of Japan (DDBJ). The mass spectrometry proteomics data have been deposited to the ProteomeXchange Consortium via the PRIDE partner repository[57] with dataset identifiers PXD058072 (related to Fig. 1 B–E and S1A, B), PXD058075 (related to and Fig. 4A,B), and PXD058080 (related to Fig. S4A–C).

Acknowledgements

This research was supported by JSPS KAKENHI (grant no. JP18K14623 and JP20K06568 to A.E., and JP23H04921 to K.T.) and AMED (grant no. JP21gm6410012 to A.E.).

Author contributions

The study was conceived by Akinori Endo, Keiji Tanaka, and Yukiko Yoshida. Transcriptome analyses were performed by Yasumasa Nishito. Proteome analyses were performed by Akinori Endo. Microscopy analyses were performed by Akinori Endo. Biochemical experiments were performed by Akinori Endo and Chikage Takahashi. Writing and editing were performed by Akinori Endo and Yukiko Yoshida.

Declaration of interest

The authors declare no competing financial interests.

REFERENCES

1. Ballabio, A., and Bonifacino, J.S. (2020). Lysosomes as dynamic regulators of cell and organismal homeostasis. Nat Rev Mol Cell Biol *21*, 101-118. 10.1038/s41580-019-0185-4.
2. Yang, C., and Wang, X. (2021). Lysosome biogenesis: Regulation and functions. J Cell Biol *220*. 10.1083/jcb.202102001.
3. Tan, J.X., and Finkel, T. (2023). Lysosomes in senescence and aging. EMBO Rep *24*, e57265. 10.15252/embr.202357265.
4. Settembre, C., and Perera, R.M. (2024). Lysosomes as coordinators of cellular catabolism, metabolic signalling and organ physiology. Nat Rev Mol Cell Biol *25*, 223-245. 10.1038/s41580-023-00676-x.
5. Bonam, S.R., Wang, F., and Muller, S. (2019). Lysosomes as a therapeutic target. Nat Rev Drug Discov *18*, 923-948. 10.1038/s41573-019-0036-1.
6. Papadopoulos, C., and Meyer, H. (2017). Detection and Clearance of Damaged Lysosomes by the Endo-Lysosomal Damage Response and Lysophagy. Curr Biol *27*, R1330-R1341. 10.1016/j.cub.2017.11.012.
7. Cantuti-Castelvetri, L., Fitzner, D., Bosch-Queralt, M., Weil, M.T., Su, M., Sen, P., Ruhwedel, T., Mitkovski, M., Trendelenburg, G., Lütjohann, D., et al. (2018). Defective cholesterol clearance limits remyelination in the aged central nervous system. Science *359*, 684-688. 10.1126/science.aan4183.
8. Mossman, B.T., and Churg, A. (1998). Mechanisms in the pathogenesis of asbestosis and silicosis. Am J Respir Crit Care Med *157*, 1666-1680. 10.1164/ajrccm.157.5.9707141.
9. Gómez-Sintes, R., Ledesma, M.D., and Boya, P. (2016). Lysosomal cell death mechanisms in aging. Ageing Res Rev *32*, 150-168. 10.1016/j.arr.2016.02.009.
10. Wang, F., Gomez-Sintes, R., and Boya, P. (2018). Lysosomal membrane permeabilization and cell death. Traffic *19*, 918-931. 10.1111/tra.12613.
11. Hornung, V., Bauernfeind, F., Halle, A., Samstad, E.O., Kono, H., Rock, K.L., Fitzgerald, K.A., and Latz, E. (2008). Silica crystals and aluminum salts activate the NALP3 inflammasome through phagosomal destabilization. Nat Immunol *9*, 847-856. 10.1038/ni.1631.
12. Nakamura, S., Shigeyama, S., Minami, S., Shima, T., Akayama, S., Matsuda, T., Esposito, A., Napolitano, G., Kuma, A., Namba-Hamano, T., et al. (2020). LC3 lipidation is essential for TFEB activation during the lysosomal damage response to kidney injury.

Nat Cell Biol *22*, 1252-1263. 10.1038/s41556-020-00583-9.

13. Meyer, H., and Kravic, B. (2024). The Endo-Lysosomal Damage Response. Annu Rev Biochem *93*, 367-387. 10.1146/annurev-biochem-030222-102505.

14. Radulovic, M., Schink, K.O., Wenzel, E.M., Nahse, V., Bongiovanni, A., Lafont, F., and Stenmark, H. (2018). ESCRT-mediated lysosome repair precedes lysophagy and promotes cell survival. EMBO J *37*. 10.15252/embj.201899753.

15. Papadopoulos, C., Kravic, B., and Meyer, H. (2020). Repair or Lysophagy: Dealing with Damaged Lysosomes. J Mol Biol *432*, 231-239. 10.1016/j.jmb.2019.08.010.

16. Eapen, V.V., Swarup, S., Hoyer, M.J., Paulo, J.A., and Harper, J.W. (2021). Quantitative proteomics reveals the selectivity of ubiquitin-binding autophagy receptors in the turnover of damaged lysosomes by lysophagy. Elife *10*. 10.7554/eLife.72328.

17. Gahlot, P., Kravic, B., Rota, G., van den Boom, J., Levantovsky, S., Schulze, N., Maspero, E., Polo, S., Behrends, C., and Meyer, H. (2024). Lysosomal damage sensing and lysophagy initiation by SPG20-ITCH. Molecular Cell. 10.1016/j.molcel.2024.02.029.

18. Chauhan, S., Kumar, S., Jain, A., Ponpuak, M., Mudd, M.H., Kimura, T., Choi, S.W., Peters, R., Mandell, M., Bruun, J.A., et al. (2016). TRIMs and Galectins Globally Cooperate and TRIM16 and Galectin-3 Co-direct Autophagy in Endomembrane Damage Homeostasis. Dev Cell *39*, 13-27. 10.1016/j.devcel.2016.08.003.

19. Koerver, L., Papadopoulos, C., Liu, B., Kravic, B., Rota, G., Brecht, L., Veenendaal, T., Polajnar, M., Bluemke, A., Ehrmann, M., et al. (2019). The ubiquitin-conjugating enzyme UBE2QL1 coordinates lysophagy in response to endolysosomal damage. EMBO Rep *20*, e48014. 10.15252/embr.201948014.

20. Yoshida, Y., Yasuda, S., Fujita, T., Hamasaki, M., Murakami, A., Kawawaki, J., Iwai, K., Saeki, Y., Yoshimori, T., Matsuda, N., and Tanaka, K. (2017). Ubiquitination of exposed glycoproteins by SCF(FBXO27) directs damaged lysosomes for autophagy. Proc Natl Acad Sci U S A *114*, 8574-8579. 10.1073/pnas.1702615114.

21. Teranishi, H., Tabata, K., Saeki, M., Umemoto, T., Hatta, T., Otomo, T., Yamamoto, K., Natsume, T., Yoshimori, T., and Hamasaki, M. (2022). Identification of CUL4A-DDB1-WDFY1 as an E3 ubiquitin ligase complex involved in initiation of lysophagy. Cell Rep *40*, 111349. 10.1016/j.celrep.2022.111349.

22. Sardiello, M., Palmieri, M., di Ronza, A., Medina, D.L., Valenza, M., Gennarino, V.A., Di Malta, C., Donaudy, F., Embrione, V., Polishchuk, R.S., et al. (2009). A gene network regulating lysosomal biogenesis and function. Science *325*, 473-477.

10.1126/science.1174447.

23. Puertollano, R., Ferguson, S.M., Brugarolas, J., and Ballabio, A. (2018). The complex relationship between TFEB transcription factor phosphorylation and subcellular localization. EMBO J *37*. 10.15252/embj.201798804.

24. Shariq, M., Khan, M.F., Raj, R., Ahsan, N., and Kumar, P. (2024). PRKAA2, MTOR, and TFEB in the regulation of lysosomal damage response and autophagy. J Mol Med (Berl) *102*, 287-311. 10.1007/s00109-023-02411-7.

25. Settembre, C., Fraldi, A., Medina, D.L., and Ballabio, A. (2013). Signals from the lysosome: a control centre for cellular clearance and energy metabolism. Nat Rev Mol Cell Biol *14*, 283-296. 10.1038/nrm3565.

26. Endo, A., Fukushima, T., Takahashi, C., Tsuchiya, H., Ohtake, F., Ono, S., Ly, T., Yoshida, Y., Tanaka, K., Saeki, Y., and Komada, M. (2024). USP8 prevents aberrant NF-kappaB and Nrf2 activation by counteracting ubiquitin signals from endosomes. J Cell Biol *223*. 10.1083/jcb.202306013.

27. Endo, A., Komada, M., and Yoshida, Y. (2024). Ubiquitin-mediated endosomal stress: A novel organelle stress of early endosomes that initiates cellular signaling pathways: USP8 serves as a gatekeeper of ubiquitin-mediated endosomal stress to counteract the activation of cellular signaling pathways. Bioessays *46*, e2400127. 10.1002/bies.202400127.

28. Jia, J., Wang, F., Bhujabal, Z., Peters, R., Mudd, M., Duque, T., Allers, L., Javed, R., Salemi, M., Behrends, C., et al. (2022). Stress granules and mTOR are regulated by membrane atg8ylation during lysosomal damage. J Cell Biol *221*. 10.1083/jcb.202207091.

29. Uchimoto, T., Nohara, H., Kamehara, R., Iwamura, M., Watanabe, N., and Kobayashi, Y. (1999). Mechanism of apoptosis induced by a lysosomotropic agent, L-Leucyl-L-Leucine methyl ester. Apoptosis *4*, 357-362. 10.1023/a:1009695221038.

30. Liberzon, A., Birger, C., Thorvaldsdottir, H., Ghandi, M., Mesirov, J.P., and Tamayo, P. (2015). The Molecular Signatures Database (MSigDB) hallmark gene set collection. Cell Syst *1*, 417-425. 10.1016/j.cels.2015.12.004.

31. Garcia-Alonso, L., Holland, C.H., Ibrahim, M.M., Turei, D., and Saez-Rodriguez, J. (2019). Benchmark and integration of resources for the estimation of human transcription factor activities. Genome Res *29*, 1363-1375. 10.1101/gr.240663.118.

32. Badia, I.M.P., Velez Santiago, J., Braunger, J., Geiss, C., Dimitrov, D., Muller-Dott, S., Taus, P., Dugourd, A., Holland, C.H., Ramirez Flores, R.O., and Saez-Rodriguez, J. (2022).

decoupleR: ensemble of computational methods to infer biological activities from omics data. Bioinform Adv *2*, vbac016. 10.1093/bioadv/vbac016.

33. Jia, J., Claude-Taupin, A., Gu, Y., Choi, S.W., Peters, R., Bissa, B., Mudd, M.H., Allers, L., Pallikkuth, S., Lidke, K.A., et al. (2020). Galectin-3 Coordinates a Cellular System for Lysosomal Repair and Removal. Dev Cell *52*, 69-87 e68. 10.1016/j.devcel.2019.10.025.

34. Kulathu, Y., Akutsu, M., Bremm, A., Hofmann, K., and Komander, D. (2009). Two-sided ubiquitin binding explains specificity of the TAB2 NZF domain. Nat Struct Mol Biol *16*, 1328-1330. 10.1038/nsmb.1731.

35. Kanayama, A., Seth, R.B., Sun, L., Ea, C.K., Hong, M., Shaito, A., Chiu, Y.H., Deng, L., and Chen, Z.J. (2004). TAB2 and TAB3 activate the NF-kappaB pathway through binding to polyubiquitin chains. Mol Cell *15*, 535-548. 10.1016/j.molcel.2004.08.008.

36. Xia, Z.P., Sun, L., Chen, X., Pineda, G., Jiang, X., Adhikari, A., Zeng, W., and Chen, Z.J. (2009). Direct activation of protein kinases by unanchored polyubiquitin chains. Nature *461*, 114-119. 10.1038/nature08247.

37. Hu, M.M., Yang, Q., Zhang, J., Liu, S.M., Zhang, Y., Lin, H., Huang, Z.F., Wang, Y.Y., Zhang, X.D., Zhong, B., and Shu, H.B. (2014). TRIM38 inhibits TNFalpha- and IL-1beta-triggered NF-kappaB activation by mediating lysosome-dependent degradation of TAB2/3. Proc Natl Acad Sci U S A *111*, 1509-1514. 10.1073/pnas.1318227111.

38. Kehl, S.R., Soos, B.A., Saha, B., Choi, S.W., Herren, A.W., Johansen, T., and Mandell, M.A. (2019). TAK1 converts Sequestosome 1/p62 from an autophagy receptor to a signaling platform. EMBO Rep *20*, e46238. 10.15252/embr.201846238.

39. Ogura, M., Shima, T., Yoshimori, T., and Nakamura, S. (2022). Protocols to monitor TFEB activation following lysosomal damage in cultured cells using microscopy and immunoblotting. STAR Protoc *3*, 101018. 10.1016/j.xpro.2021.101018.

40. Raingeaud, J., Whitmarsh, A.J., Barrett, T., Dérijard, B., and Davis, R.J. (1996). MKK3- and MKK6-regulated gene expression is mediated by the p38 mitogen-activated protein kinase signal transduction pathway. Mol Cell Biol *16*, 1247-1255. 10.1128/mcb.16.3.1247.

41. Davis, R.J. (2000). Signal transduction by the JNK group of MAP kinases. Cell *103*, 239-252. 10.1016/s0092-8674(00)00116-1.

42. Okada, M., Matsuzawa, A., Yoshimura, A., and Ichijo, H. (2014). The lysosome rupture-activated TAK1-JNK pathway regulates NLRP3 inflammasome activation. J Biol Chem *289*, 32926-32936. 10.1074/jbc.M114.579961.

43. Ben-Levy, R., Leighton, I.A., Doza, Y.N., Attwood, P., Morrice, N., Marshall, C.J., and

Cohen, P. (1995). Identification of novel phosphorylation sites required for activation of MAPKAP kinase-2. Embo j *14*, 5920-5930. 10.1002/j.1460-2075.1995.tb00280.x.

44. Wang, C., Deng, L., Hong, M., Akkaraju, G.R., Inoue, J., and Chen, Z.J. (2001). TAK1 is a ubiquitin-dependent kinase of MKK and IKK. Nature *412*, 346-351. 10.1038/35085597.

45. Tak, P.P., and Firestein, G.S. (2001). NF-kappaB: a key role in inflammatory diseases. J Clin Invest *107*, 7-11. 10.1172/JCI11830.

46. Zhong, Z., Wen, Z., and Darnell, J.E., Jr. (1994). Stat3: a STAT family member activated by tyrosine phosphorylation in response to epidermal growth factor and interleukin-6. Science *264*, 95-98. 10.1126/science.8140422.

47. Kakuda, K., Ikenaka, K., Kuma, A., Doi, J., Aguirre, C., Wang, N., Ajiki, T., Choong, C.J., Kimura, Y., Badawy, S.M.M., et al. (2024). Lysophagy protects against propagation of alpha-synuclein aggregation through ruptured lysosomal vesicles. Proc Natl Acad Sci U S A *121*, e2312306120. 10.1073/pnas.2312306120.

48. Simonaro, C.M. (2016). Lysosomes, Lysosomal Storage Diseases, and Inflammation. Journal of Inborn Errors of Metabolism and Screening *4*. 10.1177/2326409816650465.

49. Seoane, P.I., Lee, B., Hoyle, C., Yu, S., Lopez-Castejon, G., Lowe, M., and Brough, D. (2020). The NLRP3-inflammasome as a sensor of organelle dysfunction. J Cell Biol *219*. 10.1083/jcb.202006194.

50. Munoz-Planillo, R., Kuffa, P., Martinez-Colon, G., Smith, B.L., Rajendiran, T.M., and Nunez, G. (2013). K(+) efflux is the common trigger of NLRP3 inflammasome activation by bacterial toxins and particulate matter. Immunity *38*, 1142-1153. 10.1016/j.immuni.2013.05.016.

51. Zein, L., Dietrich, M., Balta, D., Bader, V., Scheuer, C., Zellner, S., Weinelt, N., Vandrey, J., Mari, M.C., Behrends, C., et al. (2023). 10.1101/2023.10.06.560832.

52. Fischer, T.D., Bunker, E.N., Zhu, P.P., Le Guerroue, F., Hadjian, M., Dominguez-Martin, E., Scavone, F., Cohen, R., Yao, T., Wang, Y., et al. (2024). STING induces HOIP-mediated synthesis of M1 ubiquitin chains to stimulate NF-kappaB signaling. EMBO J. 10.1038/s44318-024-00291-2.

53. Harding, O., Holzer, E., Riley, J.F., Martens, S., and Holzbaur, E.L.F. (2023). Damaged mitochondria recruit the effector NEMO to activate NF-kappaB signaling. Mol Cell *83*, 3188-3204 e3187. 10.1016/j.molcel.2023.08.005.

54. Demichev, V., Messner, C.B., Vernardis, S.I., Lilley, K.S., and Ralser, M. (2020). DIA-NN: neural networks and interference correction enable deep proteome coverage in high

throughput. Nat Methods *17*, 41-44. 10.1038/s41592-019-0638-x.

55. Tyanova, S., Temu, T., Sinitcyn, P., Carlson, A., Hein, M.Y., Geiger, T., Mann, M., and Cox, J. (2016). The Perseus computational platform for comprehensive analysis of (prote)omics data. Nat Methods *13*, 731-740. 10.1038/nmeth.3901.

56. Etoh, K., and Nakao, M. (2023). A web-based integrative transcriptome analysis, RNAseqChef, uncovers the cell/tissue type-dependent action of sulforaphane. J Biol Chem *299*, 104810. 10.1016/j.jbc.2023.104810.

57. Perez-Riverol, Y., Bai, J., Bandla, C., Garcia-Seisdedos, D., Hewapathirana, S., Kamatchinathan, S., Kundu, D.J., Prakash, A., Frericks-Zipper, A., Eisenacher, M., et al. (2022). The PRIDE database resources in 2022: a hub for mass spectrometry-based proteomics evidences. Nucleic Acids Res *50*, D543-D552. 10.1093/nar/gkab1038.

Figure legends

Figure 1 | Lysosomal damage has a global impact on the transcriptome and proteome

(A, B) The mean Log_2 fold change (FC, LLOMe 2 h/control) and $-Log_{10}$ P value of the transcriptome (A) and proteome (B) in RPE-1 cells are indicated on the x and y axes, respectively. Genes significantly upregulated or downregulated are labeled in red and blue, respectively.

(C) For genes showing significant upregulation in the transcriptome (Log_2 FC >1 and P <0.05), the correlation between the mean Log_2 FC of the transcriptome (from A, x axis) and the proteome (from B, y axis) is shown with a coefficient of correlation ($R = 0.5899$, $n = 302$).

(D, E) The bubble plots show the outcomes of gene enrichment analyses based on gene ontology molecular function (GOMF) (D) and MSigDB hallmark gene sets (E) for genes upregulated at the protein and RNA levels (top ten and five categories for GOMF and MSigDB hallmark gene sets, respectively). The color and size of the bubbles indicate the q value and gene ratio, respectively. The categories related to transcription, cytokine/growth factor, and apoptosis are labeled in red, blue, and green, respectively.

(F) The bubble plot illustrates the DoRothEA regulon-based prediction of transcription factors responsible for the induction of genes upregulated in cells treated with LLOMe (top five transcription factors). The color and size of the bubbles indicate the q value and gene ratio, respectively. NF-κB components are labeled in blue.

(G) Total cell lysates from RPE-1 cells treated with LLOMe for the indicated times were subjected to immunoblotting with the indicated antibodies.

(H) Schematic model of the cellular response to lysosomal damage.

Figure 2 | Lysosomal damage activates TAK1 in a ubiquitin- and TAB-dependent manner

(A) RPE-1 cells treated with LLOMe for 5 min were immunostained with the indicated antibodies and DAPI. Scale bar, 20 μm.

(B) Total cell lysates from RPE-1 cells treated with LLOMe for the indicated times were subjected to immunoblotting with the indicated antibodies.

(C) Total cell lysates from RPE-1 cells pre-treated with TAK243 for 15 min and treated with LLOMe for 15 min were subjected to immunoblotting with the indicated antibodies.

(D) Total cell lysates from RPE-1 cells transfected with the indicated siRNAs and treated with LLOMe for 15 min were subjected to immunoblotting with the indicated antibodies.

Figure 3 | The TAB–TAK1 pathway activates cytokines and transcription factors in response to lysosomal damage

(A) Heatmap showing the changes in the transcriptome of each sample. Clusters 4 and 5 include the genes upregulated by LLOMe in a TAB- and TAK1-dependent manner.

(B) The bubble plot shows the DoRothEA regulon-based prediction of transcription factors responsible for the induction of genes assigned to clusters 4 and 5 in (A) (top five transcription factors). The color and size of bubbles indicate *q* value and gene ratio, respectively. NF-κB components are labeled in blue.

(C, D) The bubble plots show the outcomes of gene enrichment analyses based on GOMF (C) and MSigDB hallmark gene sets (D) for genes assigned to clusters 4 and 5 in (A) (top five categories). The color and size of the bubbles indicate the *q* value and gene ratio, respectively. The categories related to transcription, cytokine/growth factor, and apoptosis, are labeled in red, blue, and green, respectively.

(E) Heatmaps showing the genes upregulated in a TAB- and TAK1-dependent manner within the categories of inflammatory response (left) and transcription-related factors (right). The color intensity indicates the Log_2 FC (LLOMe 2 h/control).

(F) Total cell lysates from RPE-1 cells transfected with the indicated siRNAs, treated with LLOMe for 2 h, and washed for 2 h were subjected to immunoblotting with the indicated antibodies.

Figure 4 | The K63Ub–TAB–TAK1–IKK–NF-κB pathway induces the expression of cytokines and transcription factors

(A) The mean Log_2 FC (LLOMe 30 min/control) and $-Log_{10}$ *P* value of the proteome are indicated on the x and y axes, respectively. Proteins significantly upregulated or downregulated are labeled in red and blue, respectively.

(B) IκBα protein abundance determined by mass spectrometry (MS) analysis. The individual values, mean, and standard deviation (SD) of the mean of protein abundance are presented. The mean ± SD values were calculated from two biological replicates. $^*P < 0.05$ (one-way ANOVA with Dunnett's test).

(C) Total cell lysates from RPE-1 cells treated with LLOMe for the indicated times were subjected to immunoblotting with the indicated antibodies.

(D) Total cell lysates from RPE-1 cells pre-treated with TAK243 for 15 min and treated with LLOMe for 10 min were subjected to immunoblotting with the indicated antibodies.
(E, F) Total cell lysates from RPE-1 cells transfected with the indicated siRNAs and treated with LLOMe for 10 min were subjected to immunoblotting with the indicated antibodies.
(G) Schematic model of the cellular signaling pathways activated in response to lysosomal damage.

Figure 5 | The K63Ub–TAB–TAK1–IKK–NF-κB pathway promotes cell survival and intercellular signaling

(A, B) Total RNA from RPE-1 cells pre-treated with TAK243 (A) and HS-276 (B) for 15 min and treated with LLOMe for 2 h was analyzed by RT-qPCR. Target mRNA levels were normalized to GAPDH mRNA levels; the expression levels in control cells were set to 1. The individual values, mean, and standard error of the mean (SEM) of relative mRNA levels are presented. The mean ± SEM values were calculated from three biological replicates. ****P <0.0001 (one-way ANOVA with Dunnett's test).
(C) Total RNA from RPE-1 cells transfected with the indicated siRNAs and treated with LLOMe for 2 h was analyzed by RT-qPCR. Target mRNA levels were normalized to GAPDH mRNA levels; the expression levels in cells treated with control siRNA were set to 1. The individual values, mean, and SEM of relative mRNA levels are presented. The mean ± SEM values were calculated from three biological replicates. ****P <0.0001 (one-way ANOVA with Dunnett's test).
(D) Total cell lysates from HeLa cells pre-treated with TAK243 or HS-276 for 15 min, treated with LLOMe for 2 h, and washed for 6 h were subjected to immunoblotting with the indicated antibodies.
(E, F) Total cell lysates from HeLa cells transfected with the indicated siRNAs and treated with LLOMe for 2 h, and washed for 22 h were subjected to immunoblotting with the indicated antibodies.
(G) RPE-1 cells were stimulated for the indicated times with conditioned media (CM) from RPE-1 cells treated with LLOMe for 30 min and washed for 7.5 h. Total cell lysates were subjected to immunoblotting with the indicated antibodies.
(H, I) RPE-1 cells were stimulated for 15 min with CM from RPE-1 cells transfected with the indicated siRNAs, treated with LLOMe for 30 min, and washed for 7.5 h. Total cell lysates were subjected to immunoblotting with the indicated antibodies.

1

2 **Figure 6 | Model of the ubiquitin-mediated cellular response to lysosomal damage**

3

Supplementary figure legends

Figure S1

(A) Heatmap showing genes upregulated at both the protein and mRNA levels, as derived from Fig. 1C (top 30 in proteomic upregulation). The color scale represents Log_2 FC (LLOMe 2 h/control).

(B) RNA counts (top) and protein abundance (bottom) of representative genes, as measured by RNA sequencing and MS analysis, respectively. The individual values, mean, and SEM are shown. The mean ± SEM values were calculated from three biological replicates. *P <0.05, ***P <0.001, and ****P <0.0001 (two-tailed Student's t-test).

Figure S2

(A, B) RPE-1 cells treated with LLOMe for 5 min were immunostained with the indicated antibodies and DAPI. Scale bar, 20 μm.

Figure S3

(A) Scatter plots showing the correlation between the mean Log_2 FC (LLOMe 2 h/control) in cells transfected with siControl (x axis) and siTAB2/3 (y axis) (left), and siControl (x axis) and siTAK1 (y axis) (right).

(B) Venn diagram showing the overlap of genes upregulated by LLOMe treatment in a TAB- and TAK1-dependent manner.

(C, D) The bubble plots show the outcomes of gene enrichment analyses based on GOMF (C) and MSigDB hallmark gene sets (D) for genes upregulated by LLOMe treatment in a TAB- and TAK1-dependent manner (top five categories). The color and size of the bubbles indicate the q value and gene ratio, respectively. The categories related to cytokine/growth factor and apoptosis are labeled in blue and green, respectively.

(E) RNA counts of representative genes, as measured by RNA sequencing. The individual values, mean, and SEM are presented. The mean ± SD values were calculated from three biological replicates. ****P <0.0001 (one-way ANOVA with Dunnett's test).

Figure S4

(A) The mean Log_2 FC (LLOMe 2 h/control) and $-Log_{10}$ P value of the phosphopeptides are indicated on the x and y axes, respectively. Phosphopeptides significantly upregulated or downregulated are labeled in red and blue, respectively.

(B) Correlation between the mean Log_2 FC (LLOMe 30 min/control) in cells treated with (y axis) or without HS-276 (x axis) is shown for phosphopeptides that were significantly upregulated 30 min after LLOMe treatment (Log_2 FC >1 and P <0.05).

(C) Phosphopeptides abundance measured by MS analysis. The individual values, mean, and SD of the mean of phosphopeptide abundance are shown. The mean ± SD values were calculated from three biological replicates. ****P <0.01 and *****P <0.0001 (one-way ANOVA with Dunnett's test).

Figure S5

(A) Total cell lysates from RPE-1 cells pre-treated with TAK243 or HS-276 for 15 min, treated with LLOMe for 2 h, and washed for 6 h were subjected to immunoblotting with the indicated antibodies.

Supplementary table titles

Table S1 | Transcriptome analysis LLOMe 2 h

Table S2 | Proteome analysis LLOMe 2 h

Table S3 | Correlation of Transcriptome and Proteome LLOMe 2 h

Table S4 | Transcriptome analysis RNAi LLOMe 2 h

Table S5 | Proteome analysis LLOMe 30 min

Table S6 | Phosphoproteome analysis with HS276

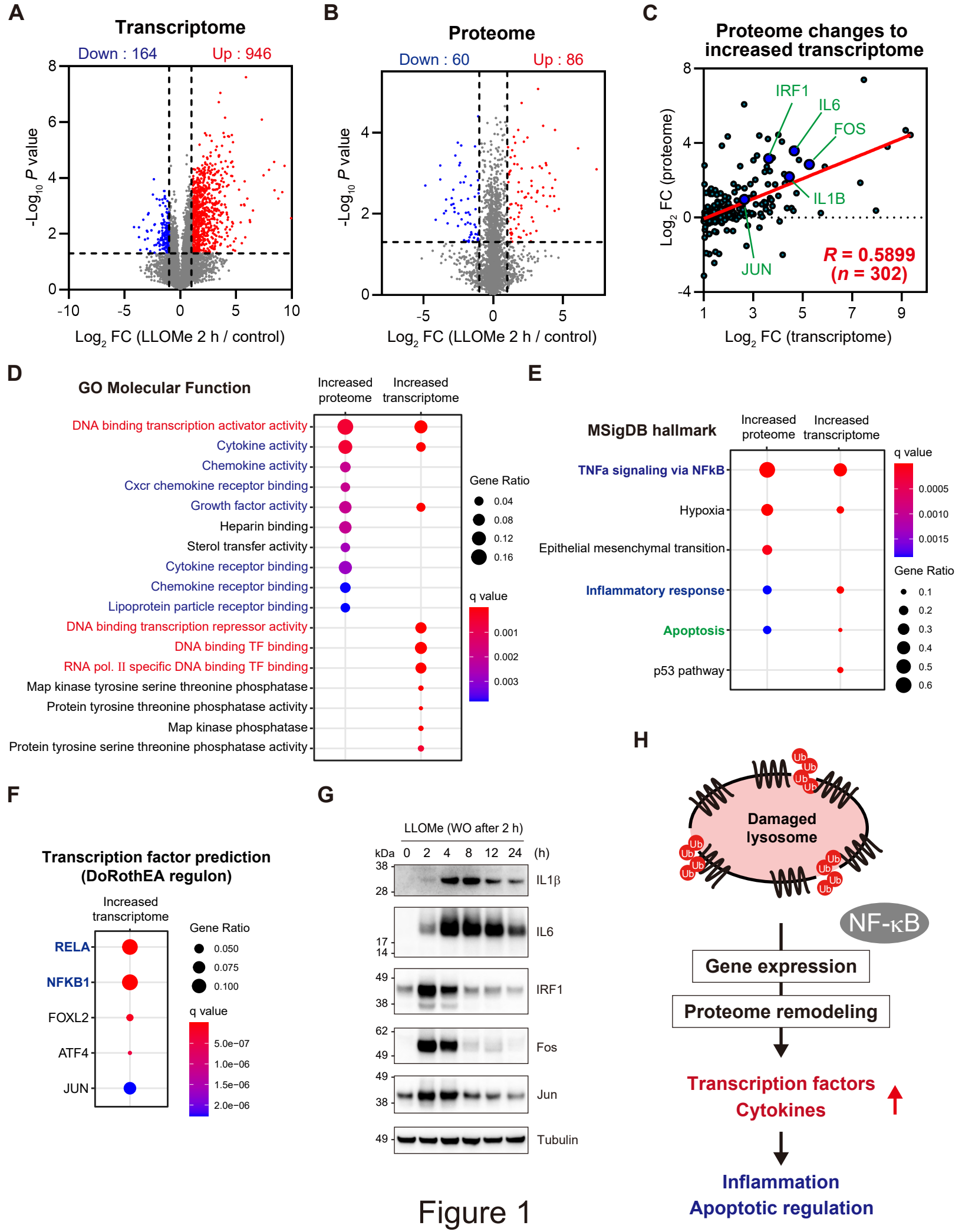
A
Transcriptome
Down : 164
Up : 946
-Log10 P value
Log2 FC (LLOMe 2 h / control)
B
Proteome
Down : 60
Up : 86
-Log10 P value
Log2 FC (LLOMe 2 h / control)
C
Proteome changes to increased transcriptome
IRF1
IL6
FOS
IL1B
JUN
R = 0.5899
(n = 302)
Log2 FC (proteome)
Log2 FC (transcriptome)
D
GO Molecular Function
Increased proteome
Increased transcriptome
DNA binding transcription activator activity
Cytokine activity
Chemokine activity
Cxcr chemokine receptor binding
Growth factor activity
Heparin binding
Sterol transfer activity
Cytokine receptor binding
Chemokine receptor binding
Lipoprotein particle receptor binding
DNA binding transcription repressor activity
DNA binding TF binding
RNA pol. II specific DNA binding TF binding
Map kinase tyrosine serine threonine phosphatase
Protein tyrosine threonine phosphatase activity
Map kinase phosphatase
Protein tyrosine serine threonine phosphatase activity
Gene Ratio
q value
E
MSigDB hallmark
Increased proteome
Increased transcriptome
TNFa signaling via NFkB
Hypoxia
Epithelial mesenchymal transition
Inflammatory response
Apoptosis
p53 pathway
q value
Gene Ratio
F
Transcription factor prediction
(DoRothEA regulon)
Increased transcriptome
RELA
NFKB1
FOXL2
ATF4
JUN
Gene Ratio
q value
G
LLOMe (WO after 2 h)
kDa 0 2 4 8 12 24 (h)
IL1β
IL6
IRF1
Fos
Jun
Tubulin
H
Damaged lysosome
Ub
NF-κB
Gene expression
Proteome remodeling
Transcription factors
Cytokines
Inflammation
Apoptotic regulation

Figure 1

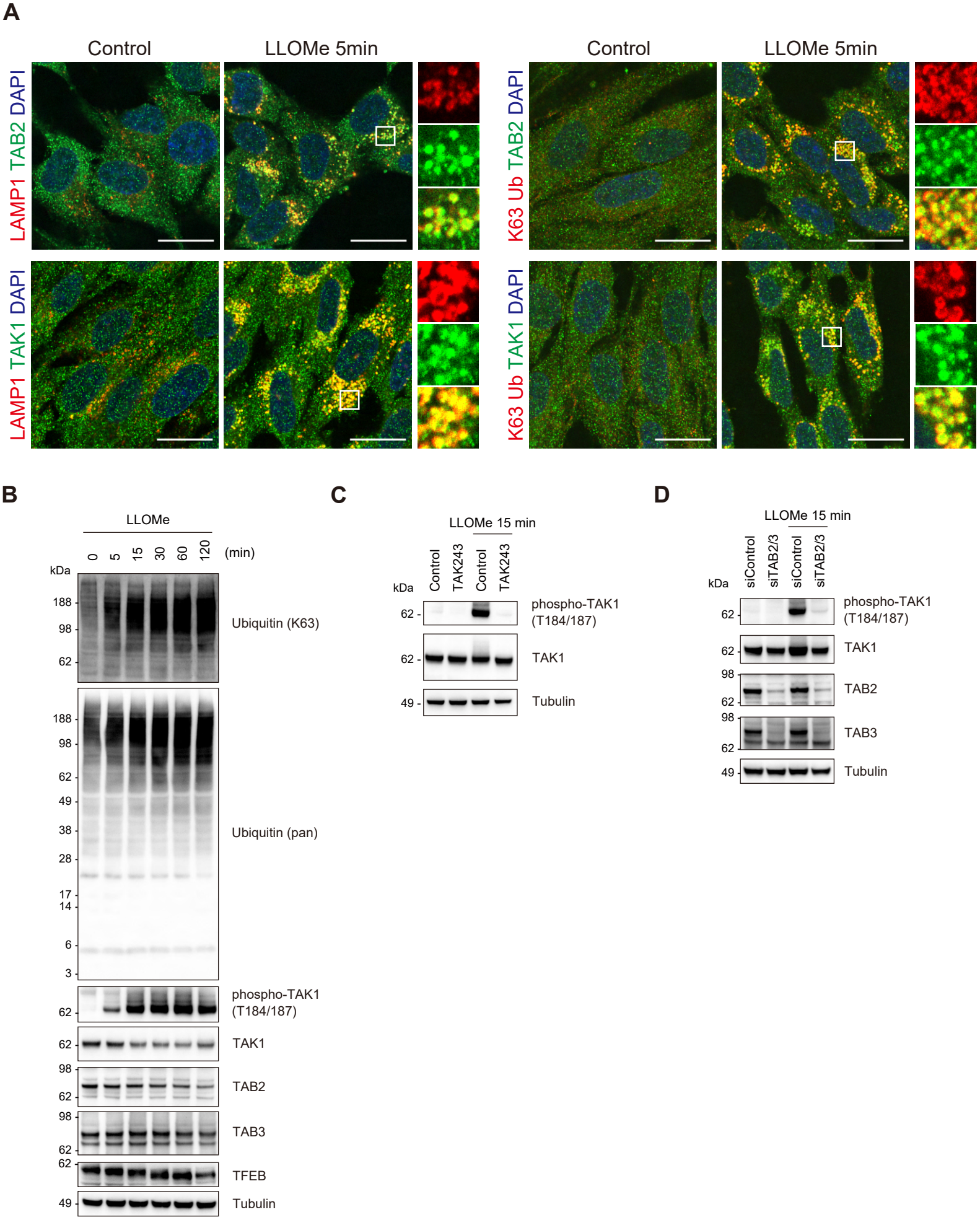
A
Control
LLOMe 5min
Control
LLOMe 5min
LAMP1 TAB2 DAPI
K63 Ub TAB2 DAPI
LAMP1 TAK1 DAPI
K63 Ub TAK1 DAPI
B
LLOMe
0
5
15
30
60
120
(min)
kDa
188
98
62
Ubiquitin (K63)
188
98
62
49
38
28
17
14
6
3
Ubiquitin (pan)
62
phospho-TAK1
(T184/187)
62
TAK1
98
62
TAB2
98
62
TAB3
62
TFEB
49
Tubulin
C
LLOMe 15 min
Control
TAK243
Control
TAK243
kDa
62
phospho-TAK1
(T184/187)
62
TAK1
49
Tubulin
D
LLOMe 15 min
siControl
siTAB2/3
siControl
siTAB2/3
kDa
62
phospho-TAK1
(T184/187)
62
TAK1
98
62
TAB2
98
62
TAB3
49
Tubulin

Figure 2

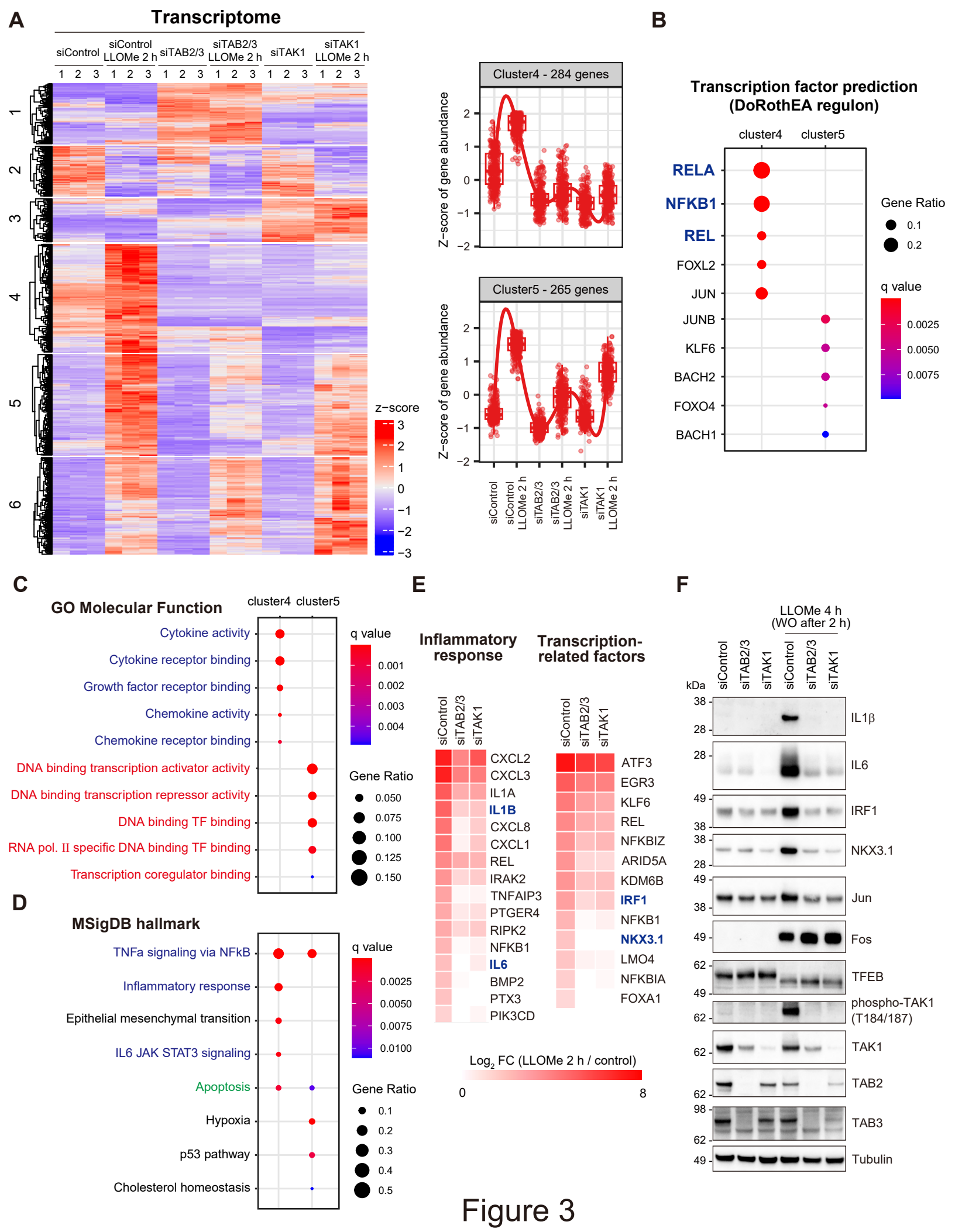
A
Transcriptome
siControl
siControl LLOMe 2 h
siTAB2/3
siTAB2/3 LLOMe 2 h
siTAK1
siTAK1 LLOMe 2 h
z−score
Cluster4 - 284 genes
Cluster5 - 265 genes
Z−score of gene abundance
B
Transcription factor prediction (DoRothEA regulon)
cluster4
cluster5
RELA
NFKB1
REL
FOXL2
JUN
JUNB
KLF6
BACH2
FOXO4
BACH1
Gene Ratio
q value
C
GO Molecular Function
Cytokine activity
Cytokine receptor binding
Growth factor receptor binding
Chemokine activity
Chemokine receptor binding
DNA binding transcription activator activity
DNA binding transcription repressor activity
DNA binding TF binding
RNA pol. II specific DNA binding TF binding
Transcription coregulator binding
D
MSigDB hallmark
TNFa signaling via NFkB
Inflammatory response
Epithelial mesenchymal transition
IL6 JAK STAT3 signaling
Apoptosis
Hypoxia
p53 pathway
Cholesterol homeostasis
E
Inflammatory response
Transcription-related factors
CXCL2
CXCL3
IL1A
IL1B
CXCL8
CXCL1
REL
IRAK2
TNFAIP3
PTGER4
RIPK2
NFKB1
IL6
BMP2
PTX3
PIK3CD
ATF3
EGR3
KLF6
REL
NFKBIZ
ARID5A
KDM6B
IRF1
NFKB1
NKX3.1
LMO4
NFKBIA
FOXA1
Log2 FC (LLOMe 2 h / control)
F
LLOMe 4 h (WO after 2 h)
kDa
IL1β
IL6
IRF1
NKX3.1
Jun
Fos
TFEB
phospho-TAK1 (T184/187)
TAK1
TAB2
TAB3
Tubulin

Figure 3

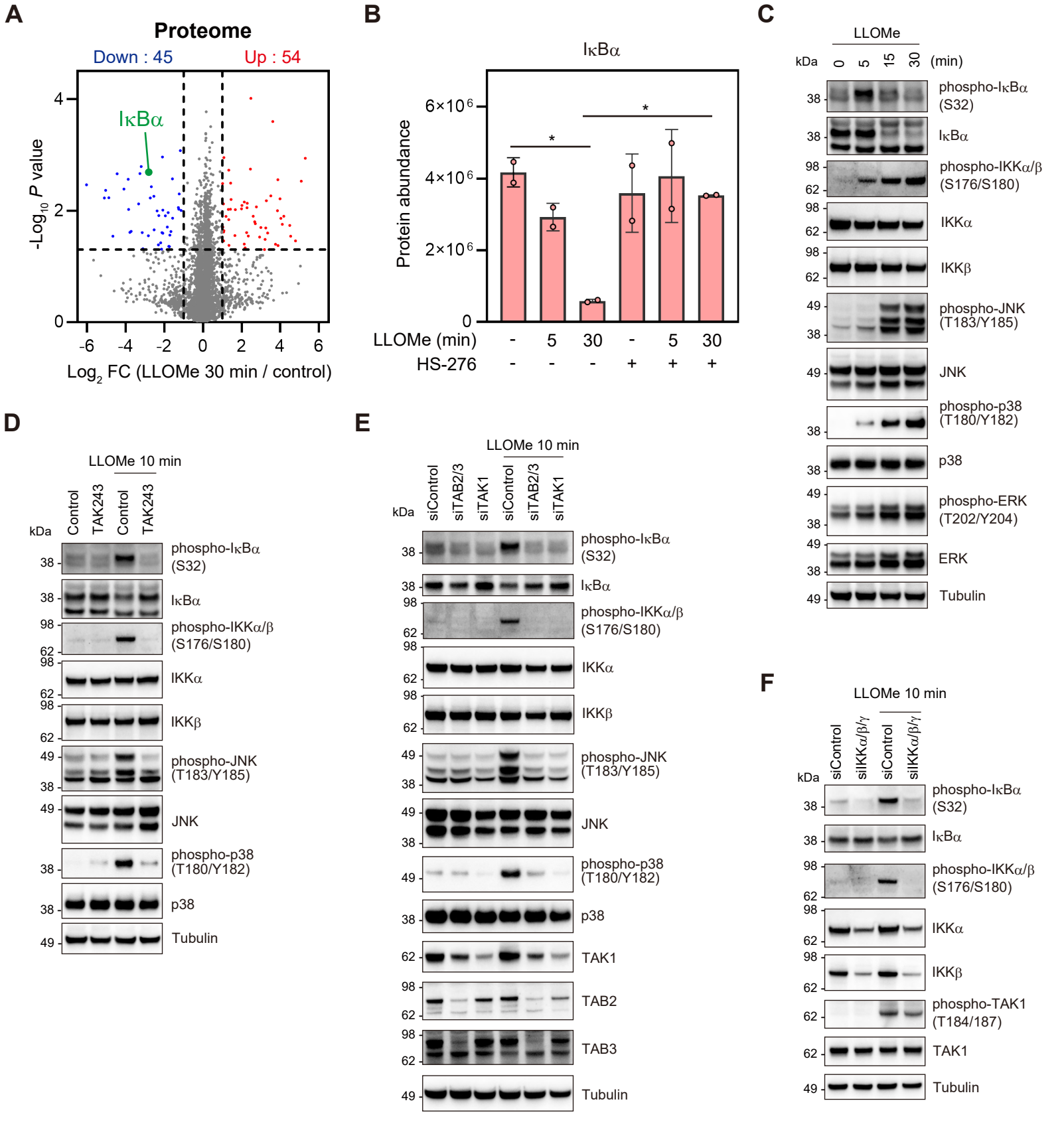
A
Proteome
Down : 45
Up : 54
IκBα
-Log10 P value
Log2 FC (LLOMe 30 min / control)
B
IκBα
Protein abundance
6×10^6
4×10^6
2×10^6
0
LLOMe (min) - 5 30 - 5 30
HS-276 - - - + + +
C
LLOMe
kDa 0 5 15 30 (min)
phospho-IκBα (S32)
IκBα
phospho-IKKα/β (S176/S180)
IKKα
IKKβ
phospho-JNK (T183/Y185)
JNK
phospho-p38 (T180/Y182)
p38
phospho-ERK (T202/Y204)
ERK
Tubulin
D
LLOMe 10 min
kDa Control TAK243 Control TAK243
phospho-IκBα (S32)
IκBα
phospho-IKKα/β (S176/S180)
IKKα
IKKβ
phospho-JNK (T183/Y185)
JNK
phospho-p38 (T180/Y182)
p38
Tubulin
E
LLOMe 10 min
kDa siControl siTAB2/3 siTAK1 siControl siTAB2/3 siTAK1
phospho-IκBα (S32)
IκBα
phospho-IKKα/β (S176/S180)
IKKα
IKKβ
phospho-JNK (T183/Y185)
JNK
phospho-p38 (T180/Y182)
p38
TAK1
TAB2
TAB3
Tubulin
F
LLOMe 10 min
kDa siControl siIKKα/β/γ siControl siIKKα/β/γ
phospho-IκBα (S32)
IκBα
phospho-IKKα/β (S176/S180)
IKKα
IKKβ
phospho-TAK1 (T184/187)
TAK1
Tubulin
G
Damaged lysosome
Ub
TAB2/3
TAK1
P
IKK
IκBα
Degradation
Activation
NF-κB

Figure 4

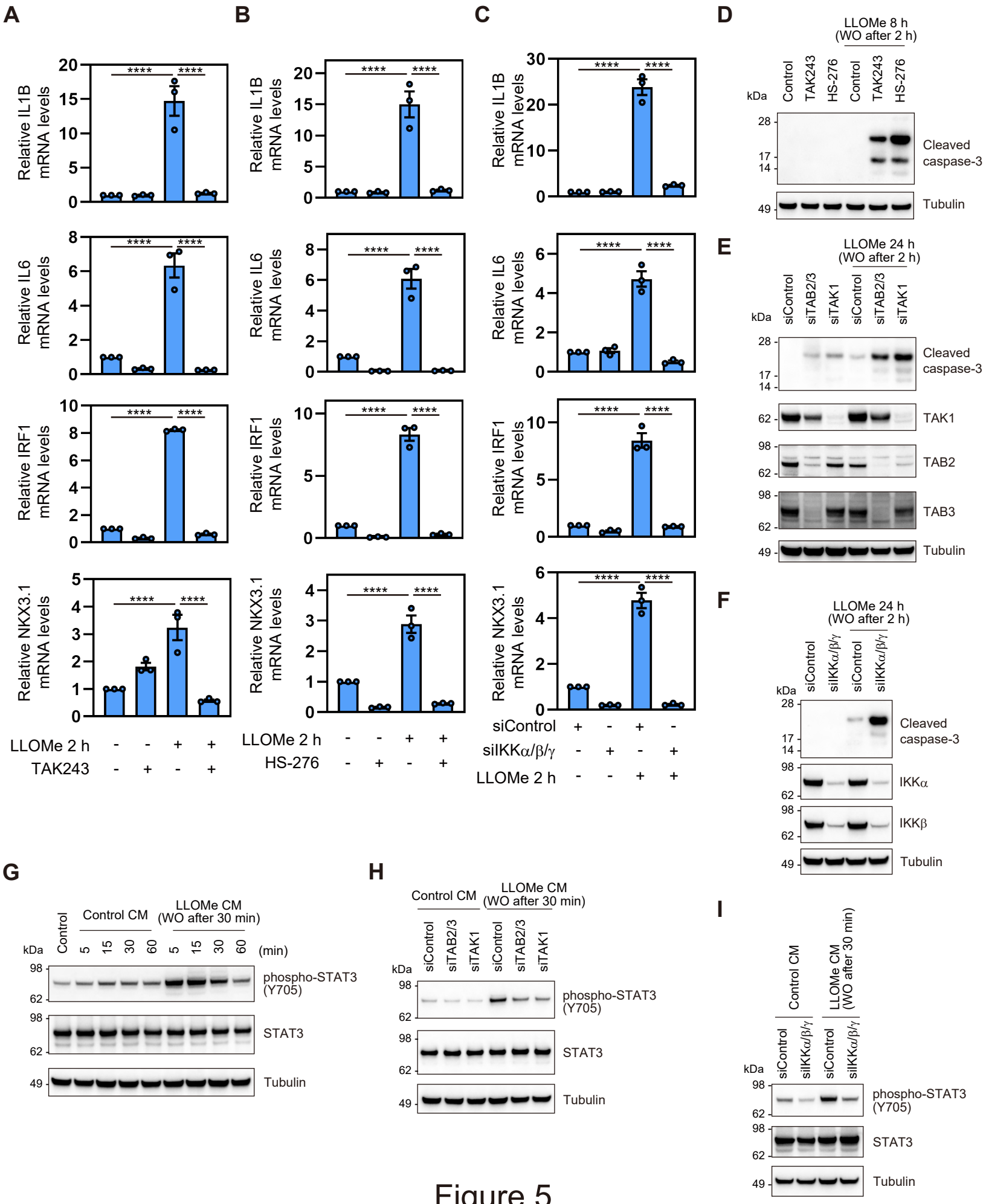
A
B
C
D
E
F
G
H
I
Relative IL1B mRNA levels
Relative IL6 mRNA levels
Relative IRF1 mRNA levels
Relative NKX3.1 mRNA levels
****
LLOMe 2 h
TAK243
HS-276
siControl
siIKKα/β/γ
LLOMe 8 h (WO after 2 h)
Control
TAK243
HS-276
kDa
Cleaved caspase-3
Tubulin
LLOMe 24 h (WO after 2 h)
siTAB2/3
siTAK1
TAK1
TAB2
TAB3
IKKα
IKKβ
Control CM
LLOMe CM (WO after 30 min)
(min)
phospho-STAT3 (Y705)
STAT3

Figure 5

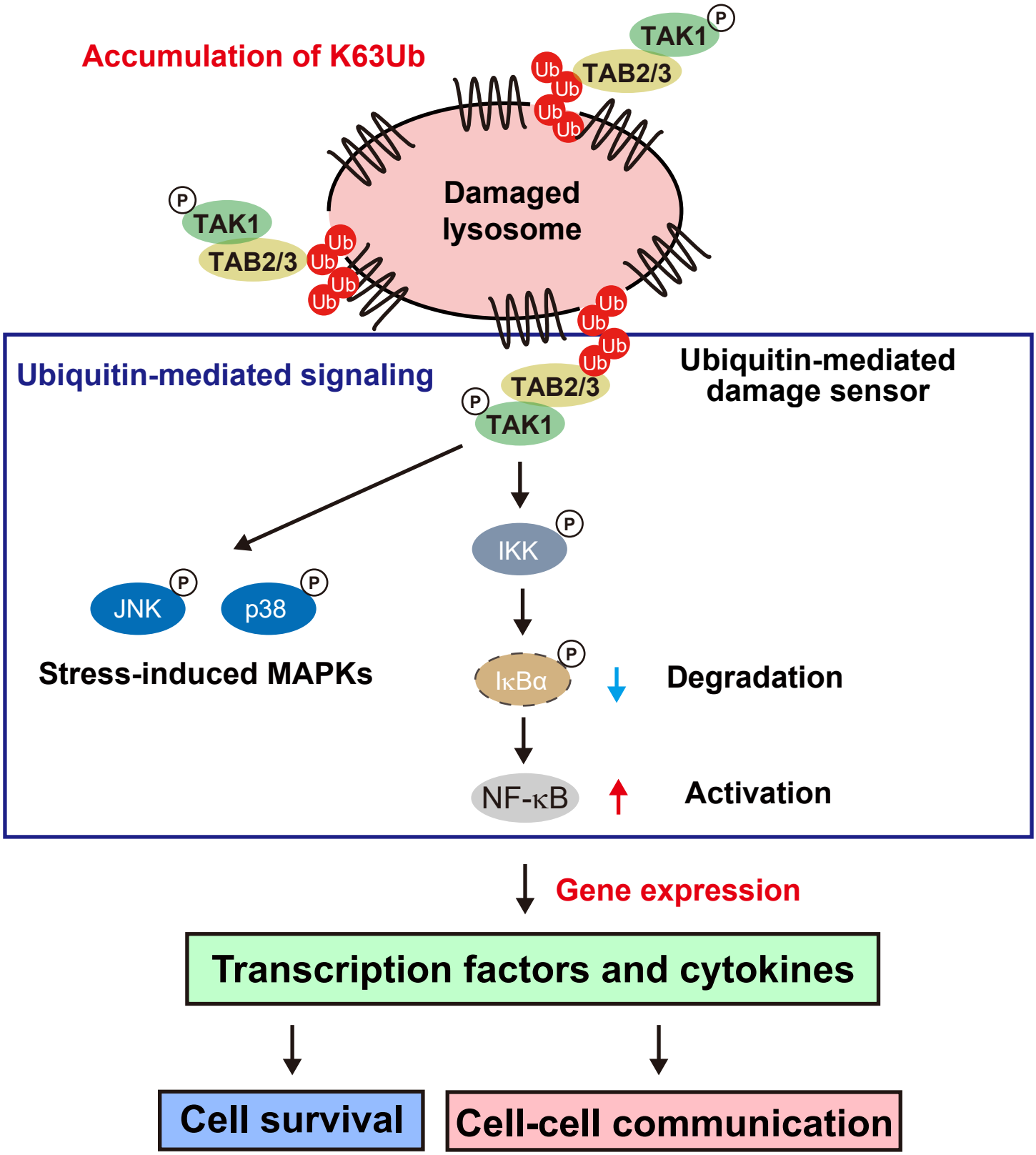
Accumulation of K63Ub
TAK1
P
TAB2/3
Ub
Damaged lysosome
Ubiquitin-mediated signaling
Ubiquitin-mediated damage sensor
IKK
JNK
p38
Stress-induced MAPKs
IκBα
Degradation
NF-κB
Activation
Gene expression
Transcription factors and cytokines
Cell survival
Cell-cell communication

Figure 6

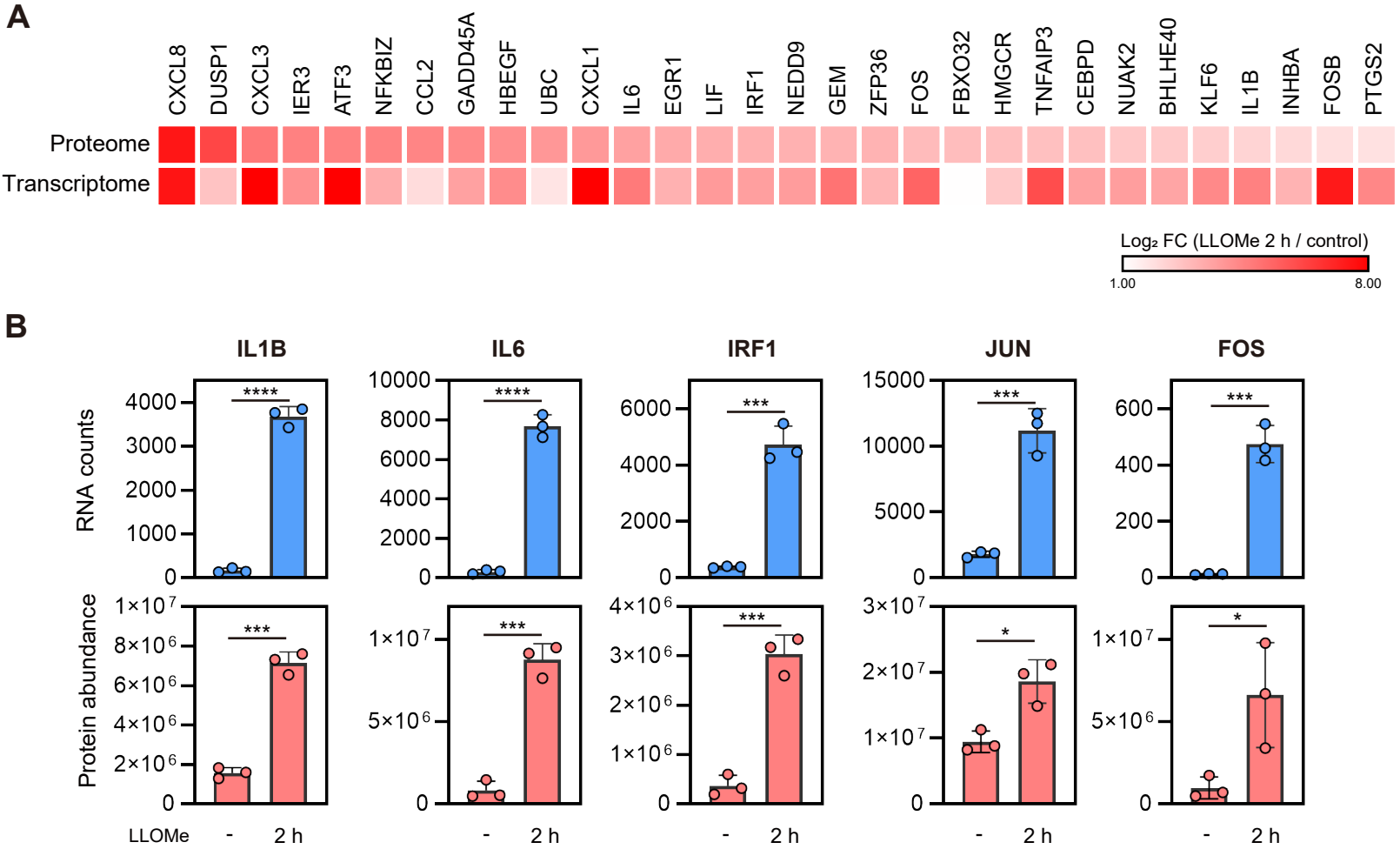

Supplement figure 1

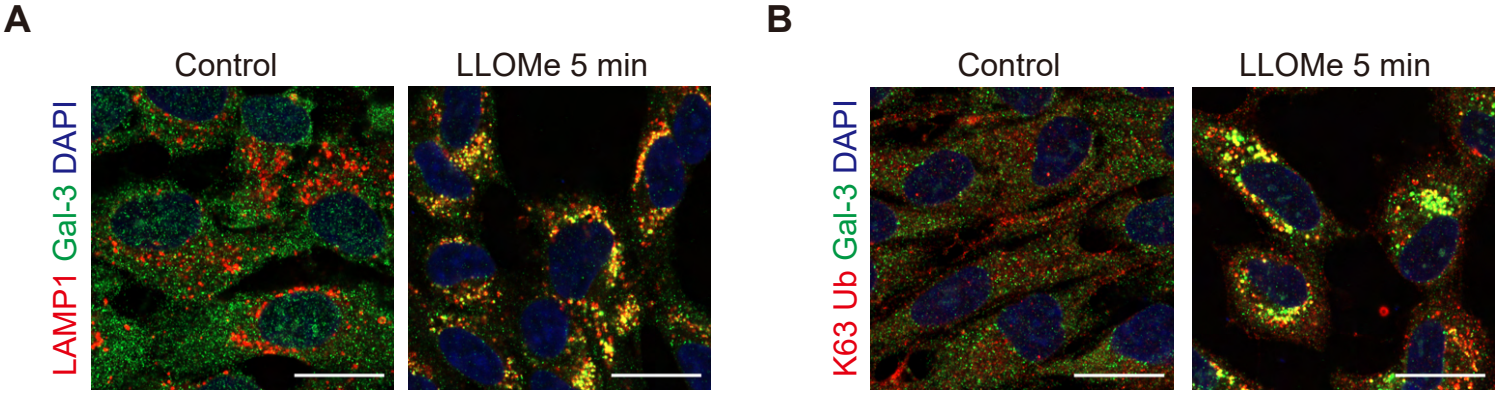

Supplement figure 2

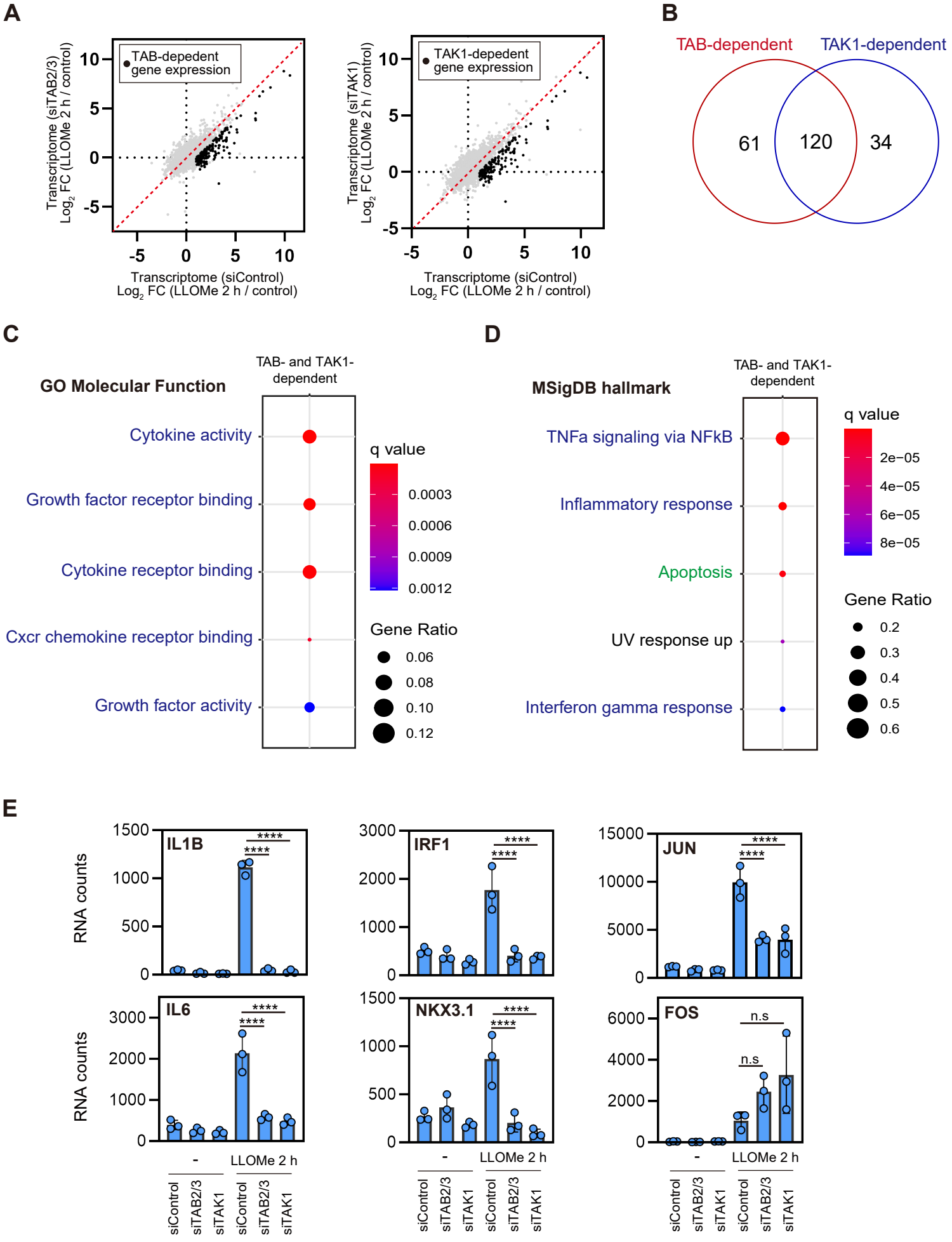

Supplement figure 3

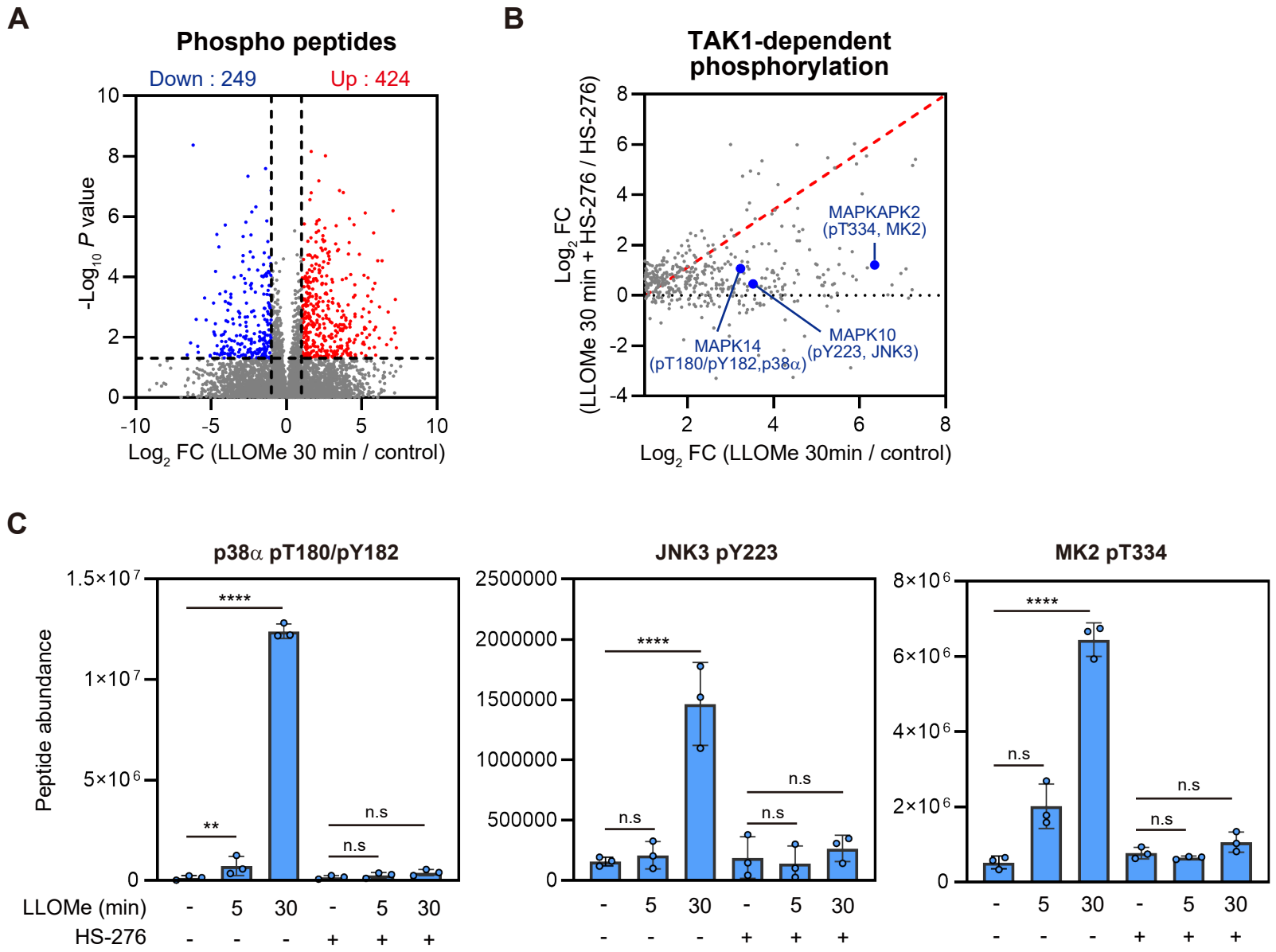

Supplement figure 4

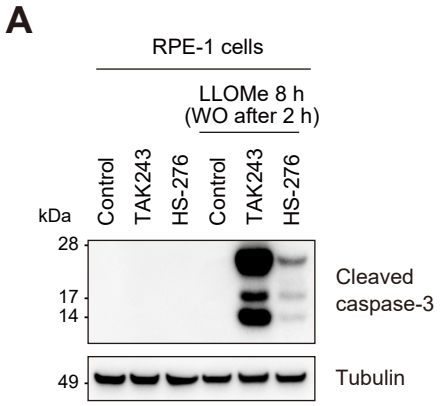

Supplement figure 5